

A Theoretical Foundation of Network Localization and Navigation

This paper provides a theoretical foundation for the design of localization and navigation networks, paving the way to a new level of performance via spatiotemporal cooperation.

BY MOE Z. WIN¹, Fellow IEEE, YUAN SHEN², Member IEEE,
AND WENHAN DAI³, Student Member IEEE

ABSTRACT | Network localization and navigation (NLN) is a promising paradigm, in which mobile nodes exploit spatiotemporal cooperation, to provide reliable location information for a diverse range of wireless applications. This paper presents a theoretical foundation of NLN, including a mathematical formulation for NLN, an introduction of equivalent Fisher information analysis, and determination of the fundamental limits of localization accuracy. Key ingredients such as spatiotemporal cooperation, array signal processing, and map exploitation are then studied. We also develop a geometric interpretation to provide insights into the essence of NLN for network design. Finally, the paper highlights the connection between the theoretical foundation and algorithm development for NLN, guiding the design and operation of practical localization systems.

KEYWORDS | Equivalent Fisher information; localization; navigation; spatiotemporal cooperation; wireless network

I. INTRODUCTION

Location awareness is essential for a wide variety of modern civil and military applications [1]–[9], such

as location-based services [10]–[12], rescue operations [13]–[15], autonomous vehicles [16]–[18], Internet-of-Things [19]–[21], health monitoring [22]–[24], and crowdsensing [25]–[27]. In outdoor environments, numerous location-based applications benefit from the meter-level positioning capability of the prominent global navigation satellite system (GNSS) technology [29]–[35]. Unfortunately, due to the weak signals from the satellites, such positioning capability becomes unreliable or even completely inaccessible in harsh propagation environments (e.g., in buildings, urban canyons, and underground) [1]–[4]. Moreover, emerging applications such as autonomous vehicles may require a higher positioning accuracy than the current GNSS technology. To address the urgent need for high-accuracy location awareness, there have been tremendous research interests and efforts from both academia and industry in recent years [36]–[53].

Localizing mobile nodes with unknown positions (called agents) can be accomplished by utilizing two types of measurements, namely, inter-node and intra-node measurements, together with prior knowledge [54]–[58]. Inter-node measurements refer to those between nodes in a network through radio-frequency (RF) transmission [59]–[63], vision sensing [64]–[66], Lidar [67]–[69], and ultrasound [70]–[72]. Typical examples of RF transmission include the relative distance, angle, or vicinity between two nodes measured by Wi-Fi, RF identification (RFID), ultrawideband (UWB), and frequency modulation (FM) radios. With the aid of a few nodes that have perfectly known positions (called anchors), inter-node measurements to these anchors can be used to estimate the agent position through multilateration or triangulation [73]–[75]. Comparatively, intra-node mea-

Manuscript received September 7, 2017; accepted April 9, 2018. Date of current version July 25, 2018. This work was supported in part by the U.S. Office of Naval Research under Grant N00014-16-1-2141; and in part by the MIT Institute for Soldier Nanotechnologies. (Corresponding author: Moe Z. Win.)

M. Z. Win is with the Laboratory for Information and Decision Systems, Massachusetts Institute of Technology, Cambridge MA 02139 USA (e-mail: win@mit.edu).

Y. Shen was with the Wireless Information and Network Sciences Laboratory, Massachusetts Institute of Technology, Cambridge, MA 02139 USA. He is now with the Department of Electronic Engineering, Tsinghua University, and Beijing National Research Center for Information Science and Technology, Beijing 100084, China (e-mail: shenyuan_ee@tsinghua.edu.cn).

W. Dai is with the Wireless Information and Network Sciences Laboratory, Massachusetts Institute of Technology, Cambridge MA 02139 USA (e-mail: whdai@mit.edu).

Digital Object Identifier 10.1109/JPROC.2018.2844553

measurements refer to those with respect to an agent itself, which do not involve interaction with other nodes. Typical examples include angular velocities and accelerations of a node obtained by inertial measurement units (IMUs) [76]–[81], or feature points in images captured by vision sensors [82]–[85]. Inertial measurements can be used to reconstruct the agent’s trajectory, while the feature points in multiple images can be used to estimate the agent movement [81]–[83]. In addition, prior knowledge about the agent positions is another source of information that benefits localization systems. For example, harnessing map information can effectively improve the localization performance in both theory and practice [86]–[90].

Commonly used signal metrics for RF-based range measurements include time-of-arrival (TOA) [91]–[97], time-difference-of-arrival (TDOA) [98]–[100], and received signal strength (RSS) [101]–[104].¹ Time-based metrics, such as TOA and TDOA, are obtained by measuring the signal propagation time between nodes, and RSS can be obtained by a low-cost energy accumulator. These metrics can be used to estimate inter-node distances together with the propagation speed or the channel fading model. Commonly used signal metrics for RF-based angle measurements include the direction-of-arrival (DOA) and the angle-of-arrival (AOA) [109]–[118]. Such metrics can be obtained by the carrier-phase difference of the signals received at an array of antennas, or directly using angular antennas [119]–[121]. With sufficient transmission power, signal bandwidth, or array aperture, these techniques can potentially achieve submeter localization accuracy [4]–[6].

The aforementioned GNSS can be considered as an RF-based localization technology, which estimates the position of a mobile user based on the TDOAs of the signals transmitted from several satellites [28]–[30]. In GNSS-challenged environments, terrestrial wireless networks are employed as a principal complement for providing positioning capability [1]–[4], where each agent is usually localized using the range and angle measurements to the base stations with known positions.

In contrast to conventional localization techniques, the network localization and navigation (NLN) paradigm proposed in [1] advocates that agents jointly infer their states (e.g., position, velocity, acceleration, etc.) by cooperative techniques in both spatial and temporal domains (see Fig. 1 for the general concept). In the spatial domain, each agent obtains information about its state relative to other nodes’ states by inter-node measurements (e.g., ranges). Spatial cooperation between agents involves exploiting the internode measurements of agent-agent pairs in addition to those of agent-anchor pairs, as well as sharing location information between agents for localization. Such cooperation has been shown to remarkably

¹As a side note, RSS can also be used as a fingerprint to match the entries in the database for localization with the aid of training [105]–[108]. However, the fingerprint-based techniques require extensive training for satisfactory localization performance.

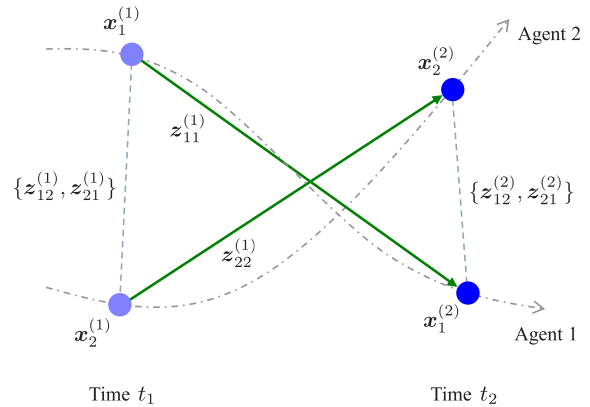


Fig. 1. An example of NLN: a network with three agents (blue circles) moving along the dashed trajectories. The empty ones denote those at time instant t_1 and the solid ones at time instant t_2 . Intra-node measurements and inter-node measurements are denoted by green and red arrows, respectively.

improve the localization performance, especially when the anchors cannot provide highquality measurements to the agents [54]–[58], [122]–[126]. To unleash the potential of spatial cooperation, there is a rich literature on the theory and algorithms in recent years [127]–[136]. In the temporal domain, each agent obtains information about its state relative to those in previous instants by intra-node measurements (e.g., accelerations). Those measurements provide the information about the state evolution over different instants and can significantly benefit localization through a filtering process [77]–[81].

Joint spatial and temporal cooperation of NLN can yield dramatic localization performance improvement over conventional approaches since additional information is exploited through cooperation with other nodes and other instants [54]–[56]. In particular, measurements among agents through cooperation contribute to the entire network from the inference point of view. However, joint spatial and temporal cooperation incurs associated costs such as additional communication and more complicated algorithms over the network: 1) the communication among nodes is required for inter-node measurements and information exchange; and 2) interdependency among the estimates of the agent positions hinders effective distributed inference algorithms [137]–[139]. Thus, to provide performance benchmarks and to guide efficient network design and operation, it is important to understand the fundamental limits of localization accuracy in NLN as well as the corresponding approaches to achieve such accuracy.² For this purpose, the information inequality can be applied to determine a lower bound for the estimation errors, which is known as the Cramér-Rao lower bound (CRLB), through the inverse of the Fisher information matrix (FIM) [140]–[143]. The CRLB is desirable for analysis in various

²For example, in designing energy-efficient localization networks, attainable localization accuracy is a meaningful performance objective.

applications due to its amenable properties and asymptotical achievability in high signal-to-noise ratio (SNR) regimes. In low SNR regimes, other bounds such as the Ziv-Zakai bound (ZZB) and Weiss-Weinstein bound (WWB) are more suitable than the CRLB but with highly complicated expressions [144]–[149].

To evaluate the localization performance in the presence of noise, CRLB-type performance bounds for certain signal metrics, e.g., time delays or AOA, are obtained in [150]–[155]. Note that the property of the signal metrics depends heavily on the signal processing procedures, and the use of certain signal metrics may discard relevant information for localization. Thus, in deriving the fundamental limits of localization accuracy, it is necessary to fully exploit the information contained in the received waveforms rather than using specific signal metrics extracted from the waveforms [156]–[158]. Based on the received wideband signals, the fundamental limits of localization accuracy for a single agent are derived in [5], and the results have been generalized to the multiple-agent scenario with spatial cooperation in [54]. In addition to spatial cooperation, temporal cooperation via intra-node measurements is incorporated in the analysis for the dynamic scenarios, where the information evolution is characterized in both spatial and temporal domains [55]. Moreover, recent studies show that the TOA and AOA information obtained from modulated signals by antenna arrays can be characterized in a unified way, where the baseband signal and the carrier signal play the role in the range and angular measurements, respectively [159].

The position inference in NLN can benefit from the availability of prior knowledge. Among others, the map information has been exploited in localization algorithms, which effectively improves the localization accuracy [86]–[88]. For map information modeled as a prior distribution, bounds such as the ZZB and WWB are more suitable than the CRLB to capture the information provided by the map. To this end, the impact of map information for localization is studied using the ZZB and WWB in [89] and [90]. The corresponding performance bounds are tighter than the CRLB in the median to low SNR regimes. These bounds give new insights into the use of map information for localization and how one should exploit such information in the localization algorithm.

This paper provides a theoretical foundation for NLN in which nodes exploit joint spatial and temporal cooperation for position inference. We determine the performance limits of a localization network employing spatial cooperation via inter-node wireless measurements, temporal cooperation via intra-node IMU measurements, as well as the prior position knowledge via map information. The main body of the paper consists of five components as follows.

- We present a general mathematical model for NLN that exploits all the position-related information (e.g., distance and angle) from the inter-node and intra-node measurements in a unified way.

- We develop the equivalent Fisher information (EFI) analysis to determine the fundamental limits of NLN and show that the location information can be decomposed into basic building blocks, each associated with a spatial or temporal measurement.
- We develop a geometric interpretation for the location information using the notion of information ellipse, by which the spatiotemporal evolution of the location information is characterized.
- We quantify the use of map information as prior knowledge for localization by the ZZB and WWB, revealing the region of SNR where the map information plays a critical role.
- We show how the theoretical foundation can guide the system design via numerical examples, through which the effects of system parameters, spatiotemporal cooperation, and the map information are quantified.

The remaining sections are organized as follows. Section II presents the system model for NLN and the methodology for EFI analysis. Section III derives the fundamental limits for noncooperative localization networks, and Section IV extends the analysis to spatiotemporal cooperative cases. Section V presents the notion of information ellipse to illustrate the behavior of the location information. Section VI discusses the use of map information in localization and introduces typical localization algorithms. Section VII presents the guidelines obtained from the theoretical foundation to network design by numerical examples. The last section draws the conclusions.

Notations: Throughout this paper, variables, vectors, and matrices are written as italic letters x , bold italic letters \mathbf{x} , and bold capital italic letters \mathbf{X} , respectively. Random variables, random vectors, and random matrices are written as sans serif letter x , bold letters \mathbf{x} , and bold capital letters \mathbf{X} , respectively. The $\mathbf{0}_m$ and $\mathbf{1}_m$ denote vectors of length m with all 0's and 1's, respectively; $[A]_{ij}$ is an element at the i th row and j th column of matrix \mathbf{A} . The notation $\mathbf{A} \succcurlyeq \mathbf{B}$ denotes that the matrix $\mathbf{A} - \mathbf{B}$ is positive semi-definite; $\text{tr}\{\mathbf{A}\}$, \mathbf{A}^T , $|\mathbf{A}|$, and $\text{adj}(\mathbf{A})$ denote the trace, transpose, determinant, and adjugate matrix of \mathbf{A} , respectively; $\|\mathbf{x}\|$ denotes the Euclidean norm of \mathbf{x} ; and \mathbb{S}_{++}^n and \mathbb{S}_+^n denote the set of $n \times n$ positive-definite and positive-semidefinite matrices, respectively. Define the unit vectors $\mathbf{u}(\varphi) := [\cos \varphi \ \sin \varphi]^T$. The notation $\mathbf{x}_{k_1:k_2}$ is used for concatenating the set of vectors $\{\mathbf{x}_{k_1}, \mathbf{x}_{k_1+1}, \dots, \mathbf{x}_{k_2}\}$, for $\{\mathbf{x}^{(t_1)}, \mathbf{x}^{(t_1+1)}, \dots, \mathbf{x}^{(t_2)}\}$, and $\mathbf{x}_{k_1:k_2}^{(t_1:t_2)}$ for $\{\mathbf{x}_{k_1:k_2}^{(t_1)}, \mathbf{x}_{k_1:k_2}^{(t_1+1)}, \dots, \mathbf{x}_{k_1:k_2}^{(t_2)}\}$ for $k_1 \leq k_2$, $t_1 \leq t_2$. The notation $\mathcal{N}(\boldsymbol{\mu}, \boldsymbol{\Sigma})$ denotes a Gaussian distribution with mean $\boldsymbol{\mu}$ and covariance matrix $\boldsymbol{\Sigma}$. We denote \otimes the Kronecker product and $\mathbf{E}_{i,j}^N$ the $N \times N$ matrix with all zeros except a 1 on the i th row and j th column.

The functions $f_{\mathbf{x}}(\mathbf{x})$, $f_{\mathbf{x}}(\mathbf{x}; \boldsymbol{\theta})$, $f_{\mathbf{x}|\mathbf{y}}(\mathbf{x}|\mathbf{y})$ denote the probability density function (PDF) of \mathbf{x} , the PDF of \mathbf{x} parameterized by $\boldsymbol{\theta}$, and the conditional PDF of \mathbf{x} given \mathbf{y} ,

respectively. We also define the functions

$$\begin{aligned}
 J_{\text{bm}}(\mathbf{z}, a(\boldsymbol{\theta}_1, \boldsymbol{\theta}_2, \boldsymbol{\theta}_3), \boldsymbol{\theta}_1, \boldsymbol{\theta}_2) &:= \frac{\partial \ln f_{\mathbf{z}}(\mathbf{z}; a(\boldsymbol{\theta}_1, \boldsymbol{\theta}_2, \boldsymbol{\theta}_3))}{\partial \boldsymbol{\theta}_1} \\
 &\quad \cdot \frac{\partial \ln f_{\mathbf{z}}(\mathbf{z}; a(\boldsymbol{\theta}_1, \boldsymbol{\theta}_2, \boldsymbol{\theta}_3))}{\partial \boldsymbol{\theta}_2^T} \\
 J_{\text{bp}}(b(\boldsymbol{\theta}_1, \boldsymbol{\theta}_2), \boldsymbol{\theta}_3, \boldsymbol{\theta}_1, \boldsymbol{\theta}_2) &:= \frac{\partial \ln f_{b(\boldsymbol{\theta}_1, \boldsymbol{\theta}_2)|\boldsymbol{\theta}_3}(b(\boldsymbol{\theta}_1, \boldsymbol{\theta}_2)|\boldsymbol{\theta}_3)}{\partial \boldsymbol{\theta}_1} \\
 &\quad \cdot \frac{\partial \ln f_{b(\boldsymbol{\theta}_1, \boldsymbol{\theta}_2)|\boldsymbol{\theta}_3}(b(\boldsymbol{\theta}_1, \boldsymbol{\theta}_2)|\boldsymbol{\theta}_3)}{\partial \boldsymbol{\theta}_2^T}.
 \end{aligned}$$

The notation $\mathbb{E}_{\mathbf{x}}\{\cdot\}$ is the expectation operator with respect to the random vector \mathbf{x} . The subscripts of f and \mathbb{E} may be omitted for brevity when clear from the context.

II. SYSTEM MODEL

This section first presents the network setting, the state model, and the measurement models for NLN, and then reviews the notion of the information inequality and the technique of the EFI analysis.

A. Network Setting

Consider a wireless network consisting of N_a agents and N_b anchors. The sets of agents and anchors are denoted by $\mathcal{N}_a = \{1, 2, \dots, N_a\}$ and $\mathcal{N}_b = \{N_a+1, N_a+2, \dots, N_a+N_b\}$, respectively. Both the measurements and inference are performed at discrete time instants t_n 's ($n = 1, 2, \dots, N$). The state of node k at time t_n is denoted by vector $\mathbf{x}_k^{(n)}$, which can include the agent position, velocity, acceleration, orientation, and angular velocity.

The goal of NLN is to determine the states of agents from inter-node and intra-node measurements as well as map information, whenever available. We denote the set of measurements made at time t_n by $\mathbf{z}^{(n)}$, which is the concatenation of vectors $\mathbf{z}_{kj}^{(n)}$, $k \in \mathcal{N}_a$, $j \in \mathcal{N}_a \cup \mathcal{N}_b$. The notations $\mathbf{z}_{kj}^{(n)}$ for $k \neq j$ represent inter-node measurements, while $\mathbf{z}_{kk}^{(n)}$ represent the intra-node measurements of agent k .

The parameter vector of the NLN problem includes the agent states and nuisance parameters associated with internode and intra-node measurements. We denote the parameter vector at time t_n by

$$\boldsymbol{\theta}^{(n)} = \left[\mathbf{x}_{1:N_a}^{(n)T} \quad \boldsymbol{\kappa}_{1:N_a}^{(n)T} \right]^T \quad (1)$$

where the measurement parameter vector $\boldsymbol{\kappa}_k^{(n)}$ is formed by the concatenation of vectors $\boldsymbol{\kappa}_{kj}^{(n)}$, $j \in \mathcal{N}_a \cup \mathcal{N}_b$, in which $\boldsymbol{\kappa}_{kj}^{(n)}$ ($k \neq j$) is associated with the inter-node measurements from node k to node j , and $\boldsymbol{\kappa}_{kk}^{(n)}$ is associated with the intra-node measurements of node k .

Note that although these measurement parameters such as clock drifts and channel amplitudes are not of interest for the NLN problem, they need to be considered since their estimation errors affect the performance of position inference. For example, the unknown clock drift will lead

to degraded intra-node velocity estimation or inter-node TOA estimation.

B. State Models

This section describes the models for the states from the non-Bayesian and Bayesian perspectives, i.e., modeling the states as deterministic unknown parameters or random parameters, respectively.

1) *Non-Bayesian Model*: The agent states and nuisance parameters associated with the measurements are modeled as deterministic unknown parameters, i.e., their prior knowledge is not available. The state $\mathbf{x}_k^{(n)}$ consists of the position and orientation of the agent k at time t_n , and the measurements $\mathbf{z}^{(n)}$ at time t_n depend on the agent positions and orientations at consecutive instants.³

Let $\boldsymbol{\theta} = \boldsymbol{\theta}^{(1:N)}$ and $\mathbf{z} = \mathbf{z}^{(1:N)}$. The likelihood function of the measurements can be written as

$$f(\mathbf{z}; \boldsymbol{\theta}) = \prod_{n=1}^N f(\mathbf{z}^{(n)}; \mathbf{x}^{(n-n_0:n)}, \boldsymbol{\kappa}^{(n)}) \quad (2)$$

where $\mathbf{x}^{(n)}$ consists of agent positions $\mathbf{p}_k^{(n)}$ and orientations $\boldsymbol{\omega}_k^{(n)}$, and the choice of n_0 depends on the type of measurements. For example, n_0 is set to 2 when the intra-node measurements $\mathbf{z}^{(n)}$ is related to agent accelerations.

Given the agent states and nuisance parameters, the measurements made by different sensors are assumed to be independent. Therefore, the measurement model in (2) can be decomposed into inter-node and intra-node measurements as

$$\begin{aligned}
 f(\mathbf{z}; \boldsymbol{\theta}) &= \prod_{n=1}^N \prod_{k \in \mathcal{N}_a} \left[\underbrace{f(\mathbf{z}_{kk}^{(n)}; \mathbf{x}_k^{(n-n_0:n)}, \boldsymbol{\kappa}_{kk}^{(n)})}_{\text{intra-node measurements}} \right. \\
 &\quad \cdot \left. \prod_{j \in \mathcal{N}_a \cup \mathcal{N}_b \setminus \{k\}} \underbrace{f(\mathbf{z}_{kj}^{(n)}; \mathbf{x}_k^{(n-n_0:n)}, \mathbf{x}_j^{(n-n_0:n)}, \boldsymbol{\kappa}_{kj}^{(n)})}_{\text{inter-node measurements}} \right]. \quad (3)
 \end{aligned}$$

2) *Bayesian Model*: In contrast to the non-Bayesian model, the agent states and nuisance parameters associated with the measurements are modeled as random variables. The dynamics of these random variables and the measurements are usually described by a hidden Markov model (HMM) [160]–[162], and the pdf of the measurements \mathbf{z} and parameters $\boldsymbol{\theta}$ is then

$$f(\mathbf{z}, \boldsymbol{\theta}) = \prod_{n=1}^N \underbrace{f(\boldsymbol{\theta}^{(n)} | \boldsymbol{\theta}^{(n-1)})}_{\text{dynamic model}} \underbrace{f(\mathbf{z}^{(n)} | \boldsymbol{\theta}^{(n)})}_{\text{measurement model}} \quad (4)$$

³For example, acceleration and angular velocity measurements can be represented by the positions and orientations of the agents at consecutive instants, as will be shown in Section II-C.

where $\theta^{(0)} := \emptyset$ is the empty set for notational convenience.

Similar to the non-Bayesian model, given the agent states and nuisance parameters, the measurements made by different sensors are assumed to be independent, and thus the measurement model can be further decomposed as

$$f(\mathbf{z}^{(n)}|\theta^{(n)}) = \prod_{k \in \mathcal{N}_a} \left[\underbrace{f(\mathbf{z}_{kk}^{(n)}|\mathbf{x}_k^{(n)}, \boldsymbol{\kappa}_{kk}^{(n)})}_{\text{intra-node measurements}} \cdot \prod_{j \in \mathcal{N}_a \cup \mathcal{N}_b \setminus \{k\}} \underbrace{f(\mathbf{z}_{kj}^{(n)}|\mathbf{x}_k^{(n)}, \mathbf{x}_j^{(n)}, \boldsymbol{\kappa}_{kj}^{(n)})}_{\text{inter-node measurements}} \right] \quad (5)$$

where $\mathbf{x}_k^{(n)}$ may include the agent positions, velocities, accelerations, orientations, and angular velocities, depending on the type of measurements.

Remark 1: In the non-Bayesian model, no prior knowledge about the dynamic evolution of the states is assumed, whereas in the Bayesian model, the dynamics of the states are modeled by an HMM via $f(\theta^{(n)}|\theta^{(n-1)})$. Moreover, in the non-Bayesian model (3), the states consist of only the node positions and orientations, and the measurements for quantities such as velocities and accelerations can be modeled by a function of the states at consecutive instants, whereas in the Bayesian model (4), the states directly include all the fundamental physical quantities related to dynamics.

While we focus on the non-Bayesian models in this paper, most results are applicable to the Bayesian models with some modifications. For several key conclusions, remarks will be included for the Bayesian models.

C. Measurement Models

We next provide the mathematical models for general inter-node and intra-node measurements based on the non-Bayesian models of the states, i.e., the state only consists of the positions and orientations.

1) *Inter-node Measurements:* The inter-node measurements, denoted by $\mathbf{z}_{kj}^{(n)}$, are performed by node k with respect to node j . Examples of such measurements include those obtained from the RF or acoustic signals transmitted from node j and received by node k , or the image of node j captured by node k 's vision sensor. In general, inter-node measurements depend only on the difference between the states of the two nodes. We next detail the relative position and velocity measurements.⁴

- **Relative position:** Node relative positions can be measured by, for example, RF or acoustic signals. Thus, by choosing $n_0 = 0$, the measurement for node relative

positions can be described as

$$\mathbf{z}_{kj}^{(n)} = \mathbf{g}_0(\mathbf{p}_k^{(n)} - \mathbf{p}_j^{(n)}, \boldsymbol{\kappa}_{kj}^{(n)}) + \mathbf{w}_{kj}^{(n)} \quad (6)$$

where $\mathbf{g}_0(\cdot)$ denotes a function of node relative positions, and $\mathbf{w}_{kj}^{(n)}$ represents the random measurement noise. The likelihood of the position measurement in (3) can then be written as

$$f(\mathbf{z}_{kj}^{(n)}; \mathbf{x}_k^{(n)}, \mathbf{x}_j^{(n)}, \boldsymbol{\kappa}_{kj}^{(n)}) = f_{\mathbf{w}_{kj}^{(n)}}(\mathbf{z}_{kj}^{(n)} - \mathbf{g}_0(\mathbf{p}_k^{(n)} - \mathbf{p}_j^{(n)}, \boldsymbol{\kappa}_{kj}^{(n)}); \mathbf{p}_k^{(n)}, \mathbf{p}_j^{(n)}, \boldsymbol{\kappa}_{kj}^{(n)}) \cdot (7)$$

- **Relative velocity:** Node relative velocities can be measured by, for example, RF or acoustic signals via the Doppler shifts. Since the velocity can be modeled as the first-order difference of node positions, by choosing $n_0 = 1$, the measurement for node relative velocities can be described as⁵

$$\mathbf{z}_{kj}^{(n)} = \mathbf{g}_1(\mathbf{p}_k^{(n)} - \mathbf{p}_k^{(n-1)} - \mathbf{p}_j^{(n)} + \mathbf{p}_j^{(n-1)}, \boldsymbol{\kappa}_{kj}^{(n)}) + \mathbf{w}_{kj}^{(n)} \quad (8)$$

where $\mathbf{g}_1(\cdot)$ denotes a function of node relative velocities. Then, the likelihood of the relative velocity measurement can be written similarly as (7).

2) *Intra-node Measurements:* The intra-node measurements, denoted by $\mathbf{z}_{kk}^{(n)}$, are performed by node k itself. Examples of such measurements include those from IMU and vision sensors. Note that the measurements related to velocities and accelerations can be modeled as a function of the agent positions and orientations at consecutive instants. Thus, the likelihood function $f(\mathbf{z}_{kk}^{(n)}; \mathbf{x}_k^{(n-n_0:n)}, \boldsymbol{\kappa}_{kk}^{(n)})$ in (3) for different types of intra-node measurements corresponds to different values of n_0 . We exemplify the likelihood function for several typical measurements in the following.

- **Position:** Node positions can be measured directly by, for example, a vision or Lidar sensor through a known local reference. Thus, by choosing $n_0 = 0$, the measurement for node positions can be described as

$$\mathbf{z}_{kk}^{(n)} = \mathbf{h}_0(\mathbf{p}_k^{(n)}, \boldsymbol{\kappa}_{kk}^{(n)}) + \mathbf{w}_k^{(n)} \quad (9)$$

where $\mathbf{h}_0(\cdot)$ denotes a function of node positions, and $\mathbf{w}_k^{(n)}$ represents the random measurement noise. Then, the likelihood of the position measurement can be written in a similar way as (7).

- **Velocity:** Node velocities are usually obtained by Doppler measurements and can be modeled as the first-order difference of node positions. Thus, by

⁴To the best of the authors' knowledge, there are no sensors yet that can directly measure the relative acceleration, relative orientation, or relative angular velocity.

⁵We reuse the notation $\mathbf{w}_{kj}^{(n)}$ as in (6) for the relative velocity measurement noise, with the understanding that it corresponds to different measurements.

choosing $n_0 = 1$, the measurement for node velocities can be described as

$$\mathbf{z}_{kk}^{(n)} = \mathbf{h}_1(\mathbf{p}_k^{(n)} - \mathbf{p}_k^{(n-1)}, \boldsymbol{\kappa}_{kk}^{(n)}) + \mathbf{w}_k^{(n)} \quad (10)$$

where $\mathbf{h}_1(\cdot)$ denotes a function of node velocities.

- **Acceleration:** Node accelerations are usually measured by an IMU and can be modeled as the secondorder difference of node positions.⁶ Thus, by choosing $n_0 = 2$, the measurement of node accelerations can be described as

$$\mathbf{z}_{kk}^{(n)} = \mathbf{h}_2(\mathbf{p}_k^{(n)} - 2\mathbf{p}_k^{(n-1)} + \mathbf{p}_k^{(n-2)}, \boldsymbol{\kappa}_{kk}^{(n)}) + \mathbf{w}_k^{(n)} \quad (11)$$

where $\mathbf{h}_2(\cdot)$ denotes a function of node accelerations.

- **Orientation:** Analogous to node positions, node orientations can be measured by a magnetometer, a vision sensor, or Lidar through a known local reference. The measurement for node orientations can be described similarly as (9) with $\mathbf{p}_k^{(n)}$ replaced by $\boldsymbol{\omega}_k^{(n)}$ and corresponding function $\mathbf{h}_0(\cdot)$.
- **Angular velocity:** Analogous to node velocities, angular velocities are usually measured by a gyroscope and can be modeled as the first-order difference of node orientations. The measurement for node angular velocities can be described similarly as (10) with $\mathbf{p}_k^{(n)}$ replaced by $\boldsymbol{\omega}_k^{(n)}$ and corresponding function $\mathbf{h}_1(\cdot)$.

3) *Special Case of Measurements:* Sections II-C1 and II-C2 have described general forms of inter-node and intranode measurements. To provide more insights into NLN, we next present the special case of the measurements that are used for developing the theoretical foundation.

We consider the inter-node measurements to be obtained by means of exchanging RF signals between the nodes in quasi-static scenarios.⁸ The wireless signal transmitted from node j and received by node k over a single-path propagation channel can be written as

$$\mathbf{z}_{kj}^{(n)}(t) = \alpha_{kj}^{(n)} s(t - \tau_{kj}^{(n)}) + \mathbf{w}_{kj}^{(n)}(t), \quad t \in [0, T_{\text{ob}}] \quad (12)$$

where $s(t)$ is a known waveform (with Fourier transform denoted by $S(f)$), $\alpha_{kj}^{(n)}$ and $\tau_{kj}^{(n)}$ are the amplitude and delay of the path, respectively, $\mathbf{w}_{kj}^{(n)}(t)$ represents the observation noise modeled as additive white Gaussian processes with two-sided power spectral density $N_0/2$, and $[0, T_{\text{ob}}]$

⁶For simplicity, we consider accelerations measured in the global coordinates here, though the measurements by IMUs are in the local coordinates.

⁷The relationship between the angular velocity and the orientation need to be treated with care for 3-D cases [76].

⁸The signal metrics, such as TOA and AOA, can be used to estimate the relative position between the nodes. With the advance of wideband transmission and array signal processing technologies, one can obtain accurate TOA and AOA measurements, which are essential for highaccuracy localization.

is the observation interval. The relationship between $\tau_{kj}^{(n)}$ and the node positions is

$$\tau_{kj}^{(n)} = \frac{1}{c} \left(\|\mathbf{p}_k^{(n)} - \mathbf{p}_j^{(n)}\| + b_{kj}^{(n)} \right) \quad (13)$$

where c is the propagation speed of the signal, and $b_{kj}^{(n)}$ denotes the range bias. The bias $b_{kj}^{(n)} = 0$ and $b_{kj}^{(n)} > 0$ for line-of-sight (LOS) and non-line-of-sight (NLOS) propagation, respectively [61].

Let $\mathbf{z}_{kj}^{(n)}$ be the vector representation of signal $\mathbf{z}_{kj}^{(n)}(t)$ obtained by the Karhunen-Loève expansion [140], and then the likelihood function of $\mathbf{z}_{kj}^{(n)}$, as a special case of (7), can be written as [5]

$$f(\mathbf{z}_{kj}^{(n)}; \mathbf{p}_k^{(n)}, \mathbf{p}_j^{(n)}, \boldsymbol{\kappa}_{kj}^{(n)}) \propto \exp \left\{ \frac{2}{N_0} \int_0^{T_{\text{ob}}} \mathbf{z}_{kj}^{(n)}(t) \alpha_{kj}^{(n)} s(t - \tau_{kj}^{(n)}) dt - \frac{1}{N_0} \int_0^{T_{\text{ob}}} [\alpha_{kj}^{(n)} s(t - \tau_{kj}^{(n)})]^2 dt \right\} \quad (14)$$

where the delay $\tau_{kj}^{(n)}$ is a function of $\mathbf{p}_k^{(n)}$ and $\mathbf{p}_j^{(n)}$ as described in (13), and the path amplitude $\alpha_{kj}^{(n)}$ and the NLOS bias $b_{kj}^{(n)}$ form the nuisance parameter vector $\boldsymbol{\kappa}_{kj}^{(n)}$.

Finally, we consider the simplest but nontrivial case for intra-node measurements, i.e., velocity measurements with additive Gaussian noises given by

$$\mathbf{z}_{kk}^{(n)} = \mathbf{p}_k^{(n)} - \mathbf{p}_k^{(n-1)} + \mathbf{w}_k^{(n)} \quad (15)$$

where $\mathbf{w}_k^{(n)} \sim \mathcal{N}(\mathbf{0}, \sigma_m^2 \mathbf{I}_2)$ in which σ_m is a known constant.

D. Information Inequality and EFI Analysis

To evaluate the performance of NLN, we first briefly review the information inequality, which gives a lower bound on the mean squared error (MSE) of estimators [140]. Consider a general measurement model $f(\mathbf{z}; \boldsymbol{\theta})$ for the observation \mathbf{z} and unknown deterministic parameter vector $\boldsymbol{\theta}$. Let $\mathbf{T}(\mathbf{z})$ be any estimator of some function of $\boldsymbol{\theta}$, denoted as $\mathbf{g}(\boldsymbol{\theta})$. Under some regularity conditions, the following information inequality holds

$$\mathbb{E} \left\{ [\mathbf{T}(\mathbf{z}) - \mathbf{g}(\boldsymbol{\theta})][\mathbf{T}(\mathbf{z}) - \mathbf{g}(\boldsymbol{\theta})]^T \right\} \succeq \frac{\partial \psi(\boldsymbol{\theta})}{\partial \boldsymbol{\theta}} \mathbf{J}_{\boldsymbol{\theta}}^{-1} \left(\frac{\partial \psi(\boldsymbol{\theta})}{\partial \boldsymbol{\theta}} \right)^T \quad (16)$$

where $\psi(\boldsymbol{\theta}) = \mathbb{E} \{ \mathbf{T}(\mathbf{z}) \}$ and

$$\mathbf{J}_{\boldsymbol{\theta}} = \mathbb{E} \{ \mathbf{J}_{\text{bm}}(\mathbf{z}, \boldsymbol{\theta}, \boldsymbol{\theta}) \} \quad (17)$$

is the FIM about $\boldsymbol{\theta}$. In particular, if $\mathbf{g}(\boldsymbol{\theta}) = \boldsymbol{\theta}$ and $\mathbf{T}(\mathbf{z})$ is an unbiased estimator, then $\psi(\boldsymbol{\theta}) = \boldsymbol{\theta}$ and (16) reduces

to [140]–[142]

$$\mathbb{E}\{[\mathbf{T}(\mathbf{z}) - \boldsymbol{\theta}][\mathbf{T}(\mathbf{z}) - \boldsymbol{\theta}]^T\} \succcurlyeq \mathbf{J}_\theta^{-1}. \quad (18)$$

In practice, only a small part of $\boldsymbol{\theta}$ may be of interest. For example, let $\boldsymbol{\theta} = [\boldsymbol{\theta}_1^T \ \boldsymbol{\theta}_2^T]^T$, where $\boldsymbol{\theta}_1$ is a vector of parameters of interest and $\boldsymbol{\theta}_2$ is a vector of nuisance parameters. Following (18), we have

$$\mathbb{E}\{[\mathbf{T}_1(\mathbf{z}) - \boldsymbol{\theta}_1][\mathbf{T}_1(\mathbf{z}) - \boldsymbol{\theta}_1]^T\} \succcurlyeq [\mathbf{J}_\theta^{-1}]_{\boldsymbol{\theta}_1} \quad (19)$$

where $\mathbf{T}_1(\mathbf{z})$ is an unbiased estimator of $\boldsymbol{\theta}_1$ and $[\mathbf{J}_\theta^{-1}]_{\boldsymbol{\theta}_1}$ denotes the square submatrix of \mathbf{J}_θ^{-1} corresponding to $\boldsymbol{\theta}_1$.

Evaluating \mathbf{J}_θ^{-1} may be complicated since $\boldsymbol{\theta}$ can be a vector of high dimensions, while only a relatively small submatrix $[\mathbf{J}_\theta^{-1}]_{\boldsymbol{\theta}_1}$ is of interest. To obtain better insights, we introduce the methodology of EFI analysis [5].

Definition 1 (EFIM): Given a parameter vector $\boldsymbol{\theta} = [\boldsymbol{\theta}_1^T \ \boldsymbol{\theta}_2^T]^T$ and the FIM \mathbf{J}_θ of the form

$$\mathbf{J}_\theta = \begin{bmatrix} \mathbf{A} & \mathbf{B} \\ \mathbf{B}^T & \mathbf{C} \end{bmatrix} \quad (20)$$

where $\boldsymbol{\theta} \in \mathbb{R}^N$, $\boldsymbol{\theta}_1 \in \mathbb{R}^n$, $\mathbf{A} \in \mathbb{R}^{n \times n}$, $\mathbf{B} \in \mathbb{R}^{n \times (N-n)}$, and $\mathbf{C} \in \mathbb{R}^{(N-n) \times (N-n)}$ with $1 \leq n < N$, the equivalent Fisher information matrix (EFIM) for $\boldsymbol{\theta}_1$ is given by

$$\mathbf{J}_e(\boldsymbol{\theta}_1) := \mathbf{A} - \mathbf{B}\mathbf{C}^{-1}\mathbf{B}^T. \quad (21)$$

Note that the EFIM $\mathbf{J}_e(\boldsymbol{\theta}_1)$ is the Schur complement of the block \mathbf{C} in the original FIM \mathbf{J}_θ [163], and it retains all the necessary information to derive the information inequality for $\boldsymbol{\theta}_1$. In other words, the EFIM can be of a much lower dimension than the original FIM without loss of information for the parameters of interest. In fact, one can verify that the right-hand side of (19) is equal to the EFIM for $\boldsymbol{\theta}_1$, i.e.,

$$[\mathbf{J}_\theta^{-1}]_{\boldsymbol{\theta}_1} = \mathbf{J}_e^{-1}(\boldsymbol{\theta}_1). \quad (22)$$

Therefore, in the context of NLN and the system model (2), by letting $\boldsymbol{\theta}_1 = \mathbf{x}$, we can obtain the EFIM for the state \mathbf{x} with the corresponding information inequality as

$$\mathbb{E}\{(\hat{\mathbf{x}} - \mathbf{x})(\hat{\mathbf{x}} - \mathbf{x})^T\} \succcurlyeq \mathbf{J}_e^{-1}(\mathbf{x}). \quad (23)$$

Moreover, the EFIM can be further applied to derive the information inequality for a certain subset of the states \mathbf{x} , such as the position of an agent at a given instant. This leads to the following definition of the position error bound.

Definition 2 (SPEB): The squared position error bound (SPEB) for the position of agent k at time t_n is defined as

$$\mathcal{P}(\mathbf{p}_k^{(n)}) := \text{tr} \left\{ \left[\mathbf{J}_e^{-1}(\mathbf{x}) \right]_{\mathbf{p}_k^{(n)}} \right\} \quad (24)$$

where $[\mathbf{J}_e^{-1}(\mathbf{x})]_{\mathbf{p}_k^{(n)}}$ denotes the submatrix of $\mathbf{J}_e^{-1}(\mathbf{x})$ corresponding to $\mathbf{p}_k^{(n)}$.

III. FUNDAMENTAL LIMITS OF LOCALIZATION ACCURACY

For ease of exposition, in this paper, we will mainly consider 2-D scenarios and assume that the inter-node measurements to be wireless signals modeled by (12) and the intra-node measurements only involve relative positions, i.e., $n_0 = 1$ in (3).⁹

In the simplified scenarios, the states are the agent positions denoted by $\mathbf{x} = \mathbf{p}_{1:N_a}^{(1:N)}$, and the inter-node and intra-node measurements are the received wireless signals $\mathbf{z}_{kj}^{(n)}(t)$ given by (12) and velocity measurements given by (15), respectively. Thus, the parameter vector at time t_n given in (1) can be written as

$$\boldsymbol{\theta}^{(n)} = [\mathbf{p}_{1:N_a}^{(n)T} \ \boldsymbol{\kappa}_{1:N_a}^{(n)T}]^T \quad (25)$$

where the nuisance parameters $\boldsymbol{\kappa}_{kk}^{(n)} = \emptyset$, and $\boldsymbol{\kappa}_{kj}^{(n)} = [\alpha_{kj}^{(n)} \ \emptyset]^T$ and $[\alpha_{kj}^{(n)} \ b_{kj}^{(n)}]^T$ for LOS and NLOS signals, respectively. In this section, we focus on the simplest case in which the agents in a static network do not cooperate with each other.¹⁰ This case essentially translates to the scenario in which $N = 1$ and $N_a = 1$. The set of measurements only consists of those between agent 1 and the anchors, i.e., $\{\mathbf{z}_{1j}\}_{j \in \mathcal{N}_b}$, and the parameters of interest are agent 1's position \mathbf{p}_1 , where the superscript is omitted for brevity as we consider only one instant.

A. Synchronous Networks

We first derive the EFIM $\mathbf{J}_e(\mathbf{p}_1)$ for agent 1's position when the agent and the anchors are all synchronized. The derivation is outlined in the following two steps. First, we show that the NLOS signals can be eliminated from the original FIM without loss of information for agent 1's position, resulting in an intermediate EFIM with a reduced dimension. Second, the channel parameters can be further eliminated by applying the EFI analysis to obtain the EFIM for agent 1's position, i.e.,

$$\begin{aligned} \mathbf{J}_\theta &= \mathbf{J}_e(\{\mathbf{p}_1, \{\boldsymbol{\kappa}_{1j}\}_{j \in \mathcal{N}_b}\}) \\ &\mapsto \mathbf{J}_e(\{\mathbf{p}_1, \{\boldsymbol{\kappa}_{1j}\}_{j \in \mathcal{N}_b, \text{los}}\}) \mapsto \mathbf{J}_e(\mathbf{p}_1) \end{aligned}$$

⁹The framework can be easily extended to multipath, dynamic, or 3-D scenarios by augmenting the state and nuisance parameter vectors to include additional parameters specific to each scenario.

¹⁰The cases of the spatiotemporal cooperation will be presented in the next section.

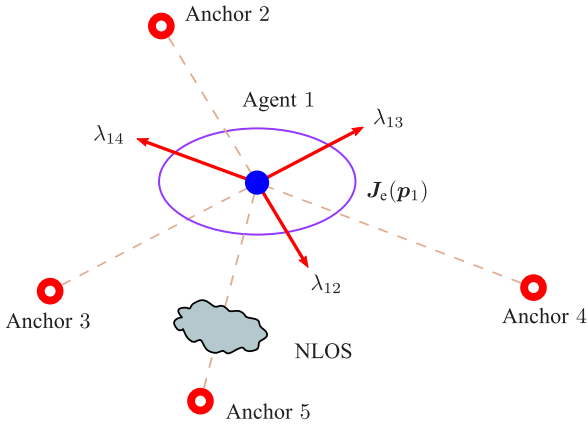


Fig. 2. A network with four anchors and one agent. Anchor 5 does not provide any RI due to NLOS propagation, while each other anchor provides agent 1 with the RI of intensity λ_{1j} along the direction from the anchor to agent 1. The purple ellipse denotes the information ellipse (described in Section V) obtained by agent 1.

where $\mathcal{N}_{b,LOS}$ and $\mathcal{N}_{b,NLOS}$ denote the sets of anchors that provide LOS and NLOS signals to agent 1, respectively. The final EFIM $\mathbf{J}_e(\mathbf{p}_1)$ is of a much lower dimension than the original FIM but retains all the necessary information for \mathbf{p}_1 .

Before stating the theorem, we introduce the notion of range information (RI) that constitutes the building blocks of the location information in two-dimensional networks as follows [5].

Definition 3 (Range Information): The RI is a 2×2 matrix of the form $\lambda \mathbf{J}_r(\phi)$, where λ is a nonnegative number called the range information intensity (RII), and $\mathbf{J}_r(\phi)$ is a 2×2 matrix called the ranging direction matrix (RDM) with angle ϕ , given by

$$\mathbf{J}_r(\phi) := \begin{bmatrix} \cos^2 \phi & \cos \phi \sin \phi \\ \cos \phi \sin \phi & \sin^2 \phi \end{bmatrix}. \quad (26)$$

Theorem 1 [5, Th. 1]: When the prior knowledge of the channel and position parameters is not available, the EFIM for agent 1's position is given by

$$\mathbf{J}_e(\mathbf{p}_1) = \sum_{j \in \mathcal{N}_{b,LOS}} \lambda_{1j} \mathbf{J}_r(\phi_{1j}) \quad (27)$$

where λ_{1j} is the RII from anchor j , given by

$$\lambda_{1j} = \frac{8\pi^2 \beta^2}{c^2} \text{SNR}_{1j} \quad (28)$$

and ϕ_{1j} is the angle from agent 1 to anchor j . In (28), β is the effective bandwidth and SNR_{1j} is the SNR of the signal, given by

$$\beta := \left(\frac{\int_{-\infty}^{+\infty} f^2 |S(f)|^2 df}{\int_{-\infty}^{+\infty} |S(f)|^2 df} \right)^{1/2} \quad (29a)$$

$$\text{SNR}_{1j} := \frac{|\alpha_{1j}|^2 \int_{-\infty}^{+\infty} |S(f)|^2 df}{N_0}. \quad (29b)$$

Remark 2: The theorem and its extensions reveal important insights into the essence of network localization, showing how the NLOS condition, multipath propagation, signal bandwidth, and network geometry affect the localization accuracy (see Fig. 2).

- **NLOS conditions:** The NLOS signals do not contribute to the EFIM for the agent position, i.e., RII $\lambda_{1j} = 0$ for $j \in \mathcal{N}_{b,NLOS}$, when there is no prior knowledge about the NLOS biases. This is because the inter-node distance obtained from the delay of the NLOS signals are corrupted by the unknown biases b_{1j} . Hence, the NLOS signals do not affect the information inequality.¹¹
- **Multipath propagation:** The EFIM (27) is also applicable to multipath propagation scenarios in which the received signal is modeled as

$$\mathbf{z}_{kj}(t) = \sum_{l=1}^L \alpha_{kj,l} s(t - \tau_{kj,l}) + \mathbf{w}_{kj}(t), \quad t \in [0, T_{ob}] \quad (30)$$

where L is the number of multipath components (MPCs), and $\alpha_{kj,l}$ and $\tau_{kj,l}$ are the amplitude and delay of the l th path, respectively. In such scenarios, the RII (28) becomes [5]

$$\lambda_{1j} = \frac{8\pi^2 \beta^2}{c^2} (1 - \chi_{1j}) \text{SNR}_{1j} \quad (31)$$

where $\chi_{1j} \in [0, 1)$, referred to as the path-overlapping coefficient, characterizes the degradation of RII due to multipath propagation. With the same SNR_{1j} of the first path, the RII for the multipath case (31) is smaller than that for the single-path case, given by (28). The degradation is caused by MPCs interfering the estimation of the arrival time of the first path. The amount of degradation is determined by the effective bandwidth of the signal $s(t)$ and the interpath delays of the MPCs in the first contiguous cluster of the received signal.¹² As a special case when the first path is resolvable from the rest of the MPCs, there is no degradation and the RII reduces to that in single-path scenarios.

- **Bandwidth:** The RII λ_{1j} is proportional to the SNR and the squared effective bandwidth of the transmitted signal $s(t)$. That is, doubling the SNR can

¹¹Nevertheless, NLOS signals can be useful in localization algorithms, e.g., resolving the ambiguity of agent positions or facilitating the search of agent positions.

¹²The first contiguous cluster [5, Def. 3], includes the MPCs that cannot be completely resolved from the first path. The path-overlapping coefficient depends on the interpath delays of the MPCs in the first contiguous cluster and is independent of their amplitudes.

reduce the SPEB by half, while doubling the effective bandwidth can reduce it by three quarters. Moreover, in connection with the effect of multipath propagation, larger bandwidth also improves the resolvability of the MPCs and reduces the degradation due to multipath propagation. Hence, it is more desirable to use ranging signals with a larger bandwidth for high-accuracy localization.

- Network geometry: While the dimension of the original FIM \mathbf{J}_θ is large,¹³ the EFIM given by (27) is a 2×2 matrix in a canonical form as a weighted sum of the RDMs from individual anchors. Anchor j can provide only 1-D RI along the direction ϕ_{1j} with intensity λ_{1j} .

In the Bayesian case, when prior knowledge of the channel parameters is available, the EFIM is also structured as a weighted sum of RDMs from individual anchors, given by¹⁴

$$\tilde{\mathbf{J}}_e(\mathbf{p}_1) = \sum_{j \in \mathcal{N}_{b, \text{LOS}}} \tilde{\lambda}_{1j} \mathbf{J}_r(\phi_{1j}) + \sum_{j \in \mathcal{N}_{b, \text{NLOS}}} \tilde{\lambda}_{1j} \mathbf{J}_r(\phi_{1j}) \quad (32)$$

where $\tilde{\lambda}_{1j}$ is the RII that incorporates prior channel knowledge. Note that the prior knowledge increases the RII of both LOS and NLOS signals, i.e., $\tilde{\lambda}_{1j}$ is always larger than or equal to the expected value of λ_{1j} in (28) over the random channel parameters. Moreover, the RII of NLOS signals can be strictly positive and contributes to the localization accuracy in contrast to the case without prior channel knowledge [5].

Furthermore, when prior knowledge of the agent position is available, the position \mathbf{p}_1 can be modeled as a random variable (RV) and the EFIM for \mathbf{p}_1 can be written as¹⁵

$$\bar{\mathbf{J}}_e(\mathbf{p}_1) = \mathbb{E}_{\mathbf{p}_1} \{ \tilde{\mathbf{J}}_e(\mathbf{p}_1) \} + \mathbf{J}_p(\mathbf{p}_1) \quad (33)$$

where the first term on the right-hand side (RHS) of (33) is the expectation of (32) over \mathbf{p}_1 , and the second term corresponds to the information from prior knowledge, given by

$$\mathbf{J}_p(\mathbf{p}_1) = \mathbb{E}_{\mathbf{p}_1} \{ \mathcal{J}_{bp}(\mathbf{p}_1, \emptyset, \mathbf{p}_1, \mathbf{p}_1) \}. \quad (34)$$

This agrees with intuition that additional information from the prior position knowledge increases the overall EFIM and thus improves the localization performance.

¹³In multipath propagation scenarios with L MPCs, the dimension of the original FIM is $2LN_b + 2$ by $2LN_b + 2$.

¹⁴In this case, the channel parameters are considered to be random and hence the parameter vector $\theta^{(n)}$ in (1) is called a hybrid parameter vector. The corresponding information inequality (16) still holds for hybrid parameter vector $\theta^{(n)}$ under some regularity conditions [144], [164].

¹⁵We denote the EFIMs with prior position knowledge by $\bar{\mathbf{J}}_e(\mathbf{p}_1)$ and $\mathbf{J}_p(\mathbf{p}_1)$ for consistency, but they are no longer functions of \mathbf{p}_1 .

The results of Theorem 1 provide the most pivotal insights of network localization, which serve as a basis for investigating more complex network scenarios and system parameters.

B. Asynchronous Networks

Note that synchronization required for high-accuracy NLN is on the order of nanoseconds, which is much more strict than that for most data communication networks (on the order of microseconds). In other words, most of the current communication infrastructures are considered to be asynchronous networks from the perspective of high-accuracy NLN.¹⁶

We next consider the scenario in which the agent is not synchronized with the anchors. This scenario can be divided into two categories: 1) the anchors are synchronized, e.g., fixed infrastructure synchronized via optical fibers; and 2) the anchors are not synchronized with each other.

In the first category, the agent can be localized via the methods of TDOA, in which the clock offset of the agent is canceled by the difference of TOAs from anchors. Denote the clock offset of agent 1 by ν_1 , and then the path delay in (13) can be written as

$$\tau_{1j} = \frac{1}{c} \left(\|\mathbf{p}_1 - \mathbf{p}_j\| + b_{1j} \right) + \nu_1, \quad j \in \mathcal{N}_b. \quad (35)$$

The clock offset of agent 1 can be incorporated into the parameter vector as

$$\boldsymbol{\theta} = [\mathbf{p}_1^T \quad \nu_1 \quad \boldsymbol{\kappa}_1^T]^T. \quad (36)$$

By applying the EFI analysis, the EFIM for agent 1's position and clock offset can be derived as

$$\mathbf{J}_e([\mathbf{p}_1^T \quad \nu_1]^T) = \sum_{j \in \mathcal{N}_{b, \text{LOS}}} \lambda_{1j} \begin{bmatrix} \mathbf{J}_r(\phi_{1j}) & c \mathbf{u}(\phi_{1j}) \\ c \mathbf{u}(\phi_{1j})^T & c^2 \end{bmatrix}. \quad (37)$$

Consequently, if we are only interested in the position estimate, the EFIM for agent 1's position can be further simplified as

$$\mathbf{J}_{e, \text{B}}(\mathbf{p}_1) = \sum_{j \in \mathcal{N}_{b, \text{LOS}}} \lambda_{1j} \mathbf{J}_r(\phi_{1j}) - \frac{1}{\sum_{j \in \mathcal{N}_{b, \text{LOS}}} \lambda_{1j}} \mathbf{u}_B \mathbf{u}_B^T \quad (38)$$

where $\mathbf{u}_B = \sum_{j \in \mathcal{N}_{b, \text{LOS}}} \lambda_{1j} \mathbf{u}(\phi_{1j})$ depends on the RII from each anchor as well as the network geometry.

Since $\mathbf{u}_B \mathbf{u}_B^T$ is a positive-semidefinite matrix and λ_{1j} 's are all positive for $j \in \mathcal{N}_{b, \text{LOS}}$, comparing (38) to (27) in

¹⁶High-accuracy NLN usually refers to submeter localization accuracy, while a clock bias of microseconds can result in localization errors on the order of hundreds of meters.

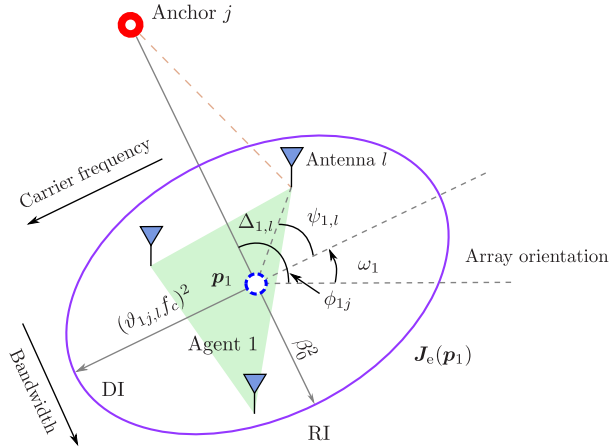


Fig. 3. Antenna array localization with unknown initial carrier phase. The location information can be decomposed into the RI and direction information (DI), which are proportional to the squared effective bandwidth of the baseband signal and the squared carrier frequency, respectively.

Theorem 1 gives

$$\mathbf{J}_{e,B}(\mathbf{p}_1) \preceq \mathbf{J}_e(\mathbf{p}_1) \quad (39)$$

where the equality is achieved only when $\mathbf{u}_B = \mathbf{0}$. The inequality (39) agrees with intuition that in general, the localization accuracy will be degraded in the asynchronous case due to the additional unknown clock offset involved in the estimation problem.

As a byproduct, the EFIM (37) also characterizes the synchronization performance of agent 1. By treating the position as nuisance parameters, the EFIM for agent 1's clock offset can be derived as

$$\mathbf{J}_e(\nu_1) = \sum_{j \in \mathcal{N}_{b,LOS}} c^2 \lambda_{1j} - c^2 \mathbf{u}_B^T \left[\sum_{j \in \mathcal{N}_{b,LOS}} \lambda_{1j} \mathbf{J}_r(\phi_{1j}) \right]^{-1} \mathbf{u}_B. \quad (40)$$

Note that the first summation in (40) is the information for synchronization when the agent position is precisely known. However, due to the location uncertainty of the agent, the synchronization performance will be degraded as expected. Indeed, the EFIM (37) characterizes the performance of joint localization and synchronization, which are coupled in wireless networks.

We now consider the second category of asynchronous networks, in which the anchors are not synchronized and thus the above TDOA methods cannot be used for localization. A feasible localization method for such a scenario is through round-trip TOA ranging [151], in which the distance between the agent and a nearby anchor is estimated using the time difference of the round-trip signal sent to and received from the anchor. For any LOS signals, the delays of the round-trip signal received by the anchor (on the anchor's clock) and received by the agent (on the

agent's clock) are given, respectively, by

$$\tau_{1j} = \frac{1}{c} \|\mathbf{p}_1 - \mathbf{p}_j\| + \nu_j, \quad \tau_{j1} = \frac{1}{c} \|\mathbf{p}_j - \mathbf{p}_1\| - \nu_j \quad (41)$$

where ν_j is the unknown clock offset between agent 1 and anchor j . Then, by using the round-trip TOA $\tau_{1j} + \tau_{j1}$,¹⁷ the clock offset can be canceled and the resulting EFIM for the agent position via round-trip TOA can be derived as

$$\mathbf{J}_{e,R}(\mathbf{p}_1) = \sum_{j \in \mathcal{N}_{b,LOS}} \frac{4\lambda_{1j}\lambda_{j1}}{\lambda_{1j} + \lambda_{j1}} \mathbf{J}_r(\phi_{1j}). \quad (42)$$

Although the structure of the EFIM (42) retains as a weighted sum of the RDMs, the effective RII is twice the harmonic mean of λ_{1j} and λ_{j1} , which is different from both the synchronized case and the first category of the asynchronous case. The reason for this phenomenon is that the ranging accuracy of the round-trip TOA depends on the delay estimation accuracy in both directions and such accuracy is limited by the worse one.

Therefore, in highly asymmetric networks such as cellular networks where the power levels of signals sent by anchors are much higher than those of the agents, the RII $\lambda_{1j} \gg \lambda_{j1}$ and thus the ranging accuracy through round-trip TOA is limited by the capability of the agents. In those cases, the EFIM in (42) can be approximated as

$$\mathbf{J}_{e,R}(\mathbf{p}_1) \approx \sum_{j \in \mathcal{N}_{b,LOS}} 4\lambda_{j1} \mathbf{J}_r(\phi_{1j}) \quad (43)$$

where only the RII λ_{j1} of the signal sent by agent 1 to anchor j is involved, and the factor of four is due to the averaging of the TOA estimates in the two directions.

C. Antenna Array Localization

So far we have focused on the simple case in which each agent is equipped with a single antenna. With the advance in multiantenna technologies, base stations and mobile devices are now widely equipped with multiple antennas for high-throughput communications. Such technologies developed primarily for communications can also be leveraged for high-accuracy localization.

Consider agent 1 equipped with an array of N_t antennas with the index set \mathcal{N}_t . The center position of the agent is denoted by \mathbf{p}_1 , while the position of the l th antenna is denoted by $\mathbf{q}_{1,l} \in \mathbb{R}^2$ for $l \in \mathcal{N}_t$. Due to the rigidity of the array, the position of each antenna can be written as a function of the center position \mathbf{p}_1 and the orientation ω_1 as (see Fig. 3)

$$\mathbf{q}_{1,l} = \mathbf{p}_1 + \Delta_{1,l} \mathbf{u}(\omega_1 + \psi_{1,l}) \quad (44)$$

¹⁷In practice, the processing time at the responder can be measured and subtracted from the total round-trip TOA at the requester for distance estimation.

where $\Delta_{1,l}$ denotes the distance between the l th antenna and the agent center, and $\psi_{1,l}$ denotes the relative direction of the l th antenna in the agent (see Fig. 3). We consider scenarios in which the distances between anchors and the agent are sufficiently larger than the array dimension such that the far-field condition applies and the channel amplitudes from an anchor to all the antennas of the agent are the same. Moreover, the phase differences between received signals in adjacent antennas are assumed to be less than 2π such that there is no periodic phase ambiguity.

Consider the transmitted signal from anchor j with a baseband signal $s_0(t)$ modulated by the carrier frequency f_c , given by

$$s_j(t) = s_0(t) \exp(i2\pi f_c t + \varsigma_j) \quad (45)$$

where $i = \sqrt{-1}$ and ς_j is the unknown initial carrier phase, which can be considered as a parameter. We assume $s_0(t)$ to be a bandlimited real signal such that its spectrum is symmetric to the origin for the ease of expressions. It can be shown that

$$\beta^2 = \beta_0^2 + f_c^2 \quad (46)$$

where β is given in (29a) and β_0 is the effective bandwidth of the baseband signal given by

$$\beta_0 := \left(\frac{\int_{-\infty}^{+\infty} f^2 |S_0(f)|^2 df}{\int_{-\infty}^{+\infty} |S_0(f)|^2 df} \right)^{1/2}. \quad (47)$$

Thus, the squared effective bandwidth of $s_j(t)$ is the sum of its baseband counterpart and the squared carrier frequency. As will be shown shortly, the two parts of the squared effective bandwidth are related to the TOA and AOA information, respectively.

Based on the array geometry in Fig. 3, the time delay of the signals (12) from anchor j at antenna l of agent 1 can be written as

$$\tau_{1j,l} = \tau_{1j} - \frac{1}{c} \Delta_{1,l} \cos(\phi_{1j} - \omega_1 - \psi_{1,l} + \tilde{\phi}_{1j}) \quad (48)$$

where ϕ_{1j} is the angle from anchor j to the center of agent 1, and $\tilde{\phi}_{1j}$ is the angle bias in the case of NLOS propagation, i.e., $\tilde{\phi}_{1j}$ is equal to 0 for $j \in \mathcal{N}_{b,LOS}$ and is unknown for $j \in \mathcal{N}_{b,NLOS}$. Then, the parameter vector of antenna array localization can be written as

$$\boldsymbol{\theta} = [\mathbf{p}_1^T \ \omega_1 \ \boldsymbol{\kappa}_1^T]^T \quad (49)$$

where the nuisance parameter vector $\boldsymbol{\kappa}_1$ consists of the amplitudes α_{1j} 's, initial carrier phase ς_j 's, and NLOS range bias b_{1j} 's as well as NLOS angle bias $\tilde{\phi}_{1j}$'s. The

measurements include the signals received at all antennas $\{\mathbf{z}_{1j,l}\}$ for $j \in \mathcal{N}_b$ and $l \in \mathcal{N}_t$.

The EFIM for agent 1's position will then be derived for the two cases: known array orientation and unknown array orientation. Before that, we define the angle variation of the l th antenna with respect to anchor j by

$$\vartheta_{1j,l} := \frac{\Delta_{1,l} \sin(\phi_{1j} - \omega_1 - \psi_{1,l})}{d_{1j}} \quad (50)$$

where $d_{1j} = \|\mathbf{p}_1 - \mathbf{p}_j\|$, and the array aperture function of agent 1 with respect to the incident angle ϕ as [159]

$$G_1(\phi) = \frac{1}{2N_t^2} \sum_{l \in \mathcal{N}_t} \sum_{m \in \mathcal{N}_t} [\Delta_{1,l} \sin(\phi - \psi_{1,l}) - \Delta_{1,m} \sin(\phi - \psi_{1,m})]^2. \quad (51)$$

Theorem 2: Given the array orientation ω_1 , the EFIM for agent 1's position is a 2×2 matrix

$$\mathbf{J}_e(\mathbf{p}_1) = \sum_{j \in \mathcal{N}_{b,LOS}} \sum_{l \in \mathcal{N}_t} \left(\lambda_{1j} \mathbf{J}_r(\phi_{1j} + \vartheta_{1j,l}) + \mu_{1j} \mathbf{J}_r(\phi_{1j} + \pi/2) \right) \quad (52)$$

where λ_{1j} and μ_{1j} are the RII and the direction information intensity (DII) from anchor j , respectively, given by

$$\lambda_{1j} = \frac{8\pi^2 \beta_0^2}{c^2} \text{SNR}_{1j} \quad (53a)$$

$$\mu_{1j} = \frac{8\pi^2 f_c^2}{c^2} \frac{G_1(\phi_{1j} - \omega_1)}{d_{1j}^2} \text{SNR}_{1j} \quad (53b)$$

in which SNR_{1j} is given by (29b).

Moreover, since $|\vartheta_{1j,l}| \approx 0$ as $d_j \gg \Delta_{1,l}$, the EFIM in (52) can be further approximated as

$$\mathbf{J}_e(\mathbf{p}_1) \approx N_t \left(\sum_{j \in \mathcal{N}_{b,LOS}} \lambda_{1j} \mathbf{J}_r(\phi_{1j}) + \mu_{1j} \mathbf{J}_r(\phi_{1j} + \pi/2) \right). \quad (54)$$

We have the following observations.

- The indexes j of both λ_{1j} and μ_{1j} belong to $\mathcal{N}_{b,LOS}$, implying that the anchors with NLOS signals provide neither RI nor DI, when there is no prior knowledge about the parameters of the NLOS signals. The reason for the latter is that the measurements of the actual AOA are corrupted by the unknown NLOS angle bias.
- The first term in the summation of (54) represents the range or TOA information from the received signals, with the RII proportional to β_0^2 along the radial angle ϕ_{1j} to anchor j . Hence, this term provides location information along the direction from the anchor to the agent, and only the baseband signal contributes to such information.

- The second term in the summation of (54) represents the direction or AOA information from the received signals, with the intensity proportional to f_c^2 along the direction perpendicular to that from the anchor to the agent. Moreover, the DII is also proportional to the “visual angle” from anchors to the array, which is equal to the array aperture function with direction $\phi_{1j} - \omega_1$ normalized by the squared distance d_{1j}^2 . The larger the aperture is, the higher the accuracy in estimating the AOA, which is consistent with classic array signal processing results [110], [112].

Remark 3: The EFIM $J_e(\mathbf{p}_1)$ is a sum of information from each agent-anchor pair, where each pair provides information along two orthogonal directions (see the ellipse in Fig. 3). Recall that the squared effective bandwidth of $s(t)$ can be decomposed as a sum of the squared effective bandwidth of the baseband signal $s_0(t)$ and the squared carrier frequency as shown in (46), and the two parts contribute to the RI and DI, respectively. Compared to the unmodulated transmission case shown in Theorem 1, the difference between (54) and (27) is due to the fact that the initial carrier phase ς_j is unknown in the modulated transmission (45). In such a case, the carrier phases cannot be used for measuring the TOA since there is an unknown initial phase in the phase measurements, and consequently only the baseband part can be exploited for TOA information. Nevertheless, the phase differences between the signals received at the array antennas can cancel out the unknown initial phase, leading to useful AOA information.

Furthermore, for the same value of effective bandwidth β , the contribution from TOA and AOA measurements to the location information depends on the partition of β into β_0 and f_c of the modulated signal (46). In traditional narrowband array localization systems, $f_c \gg \beta_0$ and hence the DI dominates the location information. In contrast, in wideband array localization systems, β_0 is comparable to f_c , and hence the RI may dominate the location information since the visual angles are usually small quantities. Therefore, in order to optimize the overall localization performance in practical systems, one may make tradeoff between the range and direction information by partitioning β_0 and f_c for a given amount of effective bandwidth.

Remark 4: In dynamic scenarios, Doppler shifts may occur due to the agent movement, which changes the carrier frequency and consequently the carrier phases of the signals received at the antenna array. In particular, the Doppler effects are shown to increase the AOA information that can be extracted from the received signals [159]. This phenomenon can be regarded as the enlargement of the virtual array aperture brought by the movement. We refer the readers to [159] for detailed discussions on the Doppler effects for antenna array localization.

Finally, we consider the case in which the array orientation ω_1 is an unknown parameter that needs to be estimated. Similar to the TDOA case in (37), the EFIM for

the position and orientation can be derived as

$$\mathbf{J}_e([\mathbf{p}_1^T \ \omega_1]^T) = \sum_{j \in \mathcal{N}_{b, \text{LOS}}} \sum_{l \in \mathcal{N}_l} \lambda_{1j} \mathbf{v}_{1j,l} \mathbf{v}_{1j,l}^T + \mu_{1j} \mathbf{w}_{1j,l} \mathbf{w}_{1j,l}^T \quad (55)$$

where

$$\begin{aligned} \mathbf{v}_{1j,l} &= [\cos(\phi_{1j} + \vartheta_{1j,l}) \quad \sin(\phi_{1j} + \vartheta_{1j,l}) \quad \vartheta_{1j,l} d_{1j}]^T \\ \mathbf{w}_{1j,l} &= [-\sin \phi_{1j} \quad \cos \phi_{1j} \quad -d_{1j}]^T. \end{aligned}$$

Then, the EFIM for the agent position can be further derived from $\mathbf{J}_e([\mathbf{p}_1^T \ \omega_1]^T)$ using the methodology of EFI analysis. It is straightforward to check that due to the additional unknown parameter, the SPEB based on (55) for the scenario with unknown orientation is higher than that based on (52) for the scenario with known orientation.

Note that when the orientation of the agent is of interest in some applications, the EFIM (55) can also be used to determine the fundamental limits of the estimation accuracy of orientations.

IV. SPATIOTEMPORAL COOPERATIVE LOCALIZATION

This section presents the fundamental limits of localization accuracy in spatiotemporal cooperative networks.

A. Spatial Cooperation

We first consider the scenario in which agents exploit spatial cooperation for localization in static networks. In this case, we have $N = 1$ but $N_a > 1$, and the set of measurements is given by $\{\mathbf{z}_{kj}\}_{k \in \mathcal{N}_a, j \in \mathcal{N}_a \cup \mathcal{N}_b \setminus \{k\}}$. The parameters of interest include all agent positions, denoted by $\mathbf{p} = \mathbf{p}_{1:N_a}$. For simplicity, we consider the synchronous case and present the EFIM for all the agents in the following theorem.¹⁸

Theorem 3: For a cooperative network with N_a agents, the EFIM for the agent positions \mathbf{p} is a $2N_a \times 2N_a$ matrix, given by

$$\mathbf{J}_e(\mathbf{p}) = \mathbf{J}_e^A(\mathbf{p}) + \mathbf{J}_e^C(\mathbf{p}) \quad (56)$$

where $\mathbf{J}_e^A(\mathbf{p})$ and $\mathbf{J}_e^C(\mathbf{p})$ representing the information from anchors and cooperation are given, respectively, by

$$\mathbf{J}_e^A(\mathbf{p}) = \sum_{k \in \mathcal{N}_a} \mathbf{E}_{k,k}^{N_a} \otimes \mathbf{J}_e^A(\mathbf{p}_k) \quad (57a)$$

$$\mathbf{J}_e^C(\mathbf{p}) = \sum_{k \in \mathcal{N}_a} \sum_{j \in \mathcal{N}_a \setminus \{k\}} (\mathbf{E}_{k,k}^{N_a} - \mathbf{E}_{k,j}^{N_a}) \otimes \mathbf{S}_{kj}. \quad (57b)$$

¹⁸The theorem directly applies to the asynchronous case of the second category, where the RII needs to be modified as in (42). However, the asynchronous case of the first category requires augmenting the dimension of the state vector with the clock offsets, and the analysis follows from those for (38).

In (57a), $\mathbf{J}_e^A(\mathbf{p}_k)$ denotes the EFIM for agent k from all anchors, given by

$$\mathbf{J}_e^A(\mathbf{p}_k) = \sum_{j \in \mathcal{N}_b} \mathbf{S}_{kj} \quad (58)$$

and \mathbf{S}_{kj} in (57b) and (58) denotes the RI from inter-node measurements, given by

$$\mathbf{S}_{kj} = \begin{cases} \lambda_{kj} \mathbf{J}_r(\phi_{kj}), & k \in \mathcal{N}_a, j \in \mathcal{N}_b \\ (\lambda_{kj} + \lambda_{jk}) \mathbf{J}_r(\phi_{kj}), & k \in \mathcal{N}_a, j \in \mathcal{N}_a \setminus \{k\} \end{cases} \quad (59)$$

where the RII λ_{kj} is given by (28) and ϕ_{kj} is the angle from node k to node j .

Remark 5: The structure of the EFIM in (56) can be expressed explicitly as (60), shown at the bottom of the page. When a particular set of agents are of interest, one can apply the EFI analysis again on their positions by treating the positions of other agents as nuisance parameters.

Building upon the insights for the noncooperative scenario described in Section III, we draw additional insights for the spatial cooperation among the agents.

- The EFIM $\mathbf{J}_e(\mathbf{p})$ for all the agents can be decomposed into location information from anchors $\mathbf{J}_e^A(\mathbf{p})$ and that from agents' cooperation $\mathbf{J}_e^C(\mathbf{p})$. The matrix $\mathbf{J}_e^A(\mathbf{p})$ is block-diagonal, where each block $\mathbf{J}_e^A(\mathbf{p}_k)$ is of size 2×2 corresponding to the location information of agent k . As in the noncooperative case, each block is a weighted sum of RDMs over anchors. Hence, the location information from anchors is not inter-related among agents. The matrix $\mathbf{J}_e^C(\mathbf{p})$ is a highly structured, consisting of RI \mathbf{S}_{kj} 's, which implies that the location information from agents' cooperation results in interrelated position estimation. In other words, the inter-node measurements provide relative location information among the agents, which needs to be jointly exploited by the agents for localization.
- The RI \mathbf{S}_{kj} is the basic building block of the overall EFIM $\mathbf{J}_e(\mathbf{p})$. Each block corresponds to a received waveform, either between an anchor and an agent, or between two agents, and the RII λ_{kj} is determined by the power and effective bandwidth of the signal, the multipath propagation channel, and the prior knowledge of the channel if available. Moreover, agents' cooperation also provide only 1-D information, as in

the case for range measurements between anchors and agents, for localization along the direction connecting the two agents.

In the Bayesian case, when prior knowledge of the agent positions is available, another component that characterizes such knowledge appears in the overall EFIM $\bar{\mathbf{J}}_e(\mathbf{p})$, such that

$$\bar{\mathbf{J}}_e(\mathbf{p}) = \mathbb{E}_{\mathbf{p}} \{ \mathbf{J}_e(\mathbf{p}) \} + \mathbf{J}_p(\mathbf{p}) \quad (61)$$

where the first component is the expectation of (56) over \mathbf{p} , and the second term represents the information from prior knowledge, given by

$$\mathbf{J}_p(\mathbf{p}) = \mathbb{E} \{ \mathbf{J}_{bp}(\mathbf{p}, \emptyset, \mathbf{p}, \mathbf{p}) \}. \quad (62)$$

It was shown in [54] that agents can be thought of as anchors if prior knowledge of the agent positions is infinite. This view can significantly facilitate the design and analysis of cooperative localization by treating the information coming from anchors and agents in a unified way.

A final comment on Theorem 3 is that if the agents do not cooperate, $\mathbf{J}_e^C(\mathbf{p}) = \mathbf{0}$ and hence $\mathbf{J}_e(\mathbf{p}) = \mathbf{J}_e^A(\mathbf{p})$ becomes a block-diagonal matrix, which reduces to the noncooperative case as expected. Thus, Theorem 3 can be viewed as a generalized form encompassing both noncooperative and cooperative cases.

B. Spatiotemporal Cooperation

Finally, we consider dynamic scenarios that incorporate the intra-node measurements from temporal cooperation. Now we have both $N > 1$ and $N_a > 1$, and the set of measurements includes all the spatial and temporal ones, denoted by $\{\mathbf{z}_{kj}^{(n)}\}_{k \in \mathcal{N}_a, j \in \mathcal{N}_a \cup \mathcal{N}_b}$. The parameters of interest include the positions of all agents at all instants, i.e., $\mathbf{p} = \mathbf{p}_{1:N_a}^{(1:N)}$, and the EFIM for \mathbf{p} can be obtained through the EFI analysis shown in the following theorem.

Theorem 4: The EFIM for the agent positions \mathbf{p} from time t_1 to t_N is a $2NN_a \times 2NN_a$ matrix written as

$$\mathbf{J}_e(\mathbf{p}) = \mathbf{J}_e^s(\mathbf{p}) + \mathbf{J}_e^t(\mathbf{p}) \quad (63)$$

where $\mathbf{J}_e^s(\mathbf{p})$ and $\mathbf{J}_e^t(\mathbf{p})$ are the EFIM corresponding to spatial and temporal cooperation, given,

$$\mathbf{J}_e(\mathbf{p}) = \begin{bmatrix} \mathbf{J}_e^A(\mathbf{p}_1) + \sum_{j \in \mathcal{N}_a \setminus \{1\}} \mathbf{S}_{1,j} & -\mathbf{S}_{1,2} & \cdots & -\mathbf{S}_{1,N_a} \\ -\mathbf{S}_{1,2} & \mathbf{J}_e^A(\mathbf{p}_2) + \sum_{j \in \mathcal{N}_a \setminus \{2\}} \mathbf{S}_{2,j} & & -\mathbf{S}_{2,N_a} \\ \vdots & & \ddots & \\ -\mathbf{S}_{1,N_a} & -\mathbf{S}_{2,N_a} & & \mathbf{J}_e^A(\mathbf{p}_{N_a}) + \sum_{j \in \mathcal{N}_a \setminus \{N_a\}} \mathbf{S}_{N_a,j} \end{bmatrix} \quad (60)$$

respectively, by¹⁹

$$\mathbf{J}_e^s(\mathbf{p}) = \sum_{n=1}^N \mathbf{E}_{n,n}^N \otimes \mathbf{S}^{(n)} \quad (64a)$$

$$\begin{aligned} \mathbf{J}_e^t(\mathbf{p}) &= \sum_{n=1}^N \mathbf{E}_{n,n}^N \otimes (\mathbf{T}^{(n)} + \mathbf{T}^{(n+1)}) \\ &\quad - \sum_{n=1}^N (\mathbf{E}_{n,n+1}^N + \mathbf{E}_{n+1,n}^N) \otimes \mathbf{T}^{(n)}. \end{aligned} \quad (64b)$$

In (64a), $\mathbf{S}^{(n)} \in \mathbb{S}_{++}^{2N_a}$ is given by

$$\begin{aligned} \mathbf{S}^{(n)} &= \sum_{k \in \mathcal{N}_a} \sum_{j \in \mathcal{N}_a \cup \mathcal{N}_b \setminus \{k\}} \mathbf{E}_{k,k}^{N_a} \otimes \mathbf{S}_{kj}^{(n)} \\ &\quad - \sum_{k \in \mathcal{N}_a} \sum_{j \in \mathcal{N}_a \setminus \{k\}} \mathbf{E}_{k,j}^{N_a} \otimes \mathbf{S}_{kj}^{(n)} \end{aligned} \quad (65)$$

with

$$\mathbf{S}_{kj}^{(n)} = \begin{cases} \lambda_{kj}^{(n)} \mathbf{J}_r(\phi_{kj}^{(n)}), & j \in \mathcal{N}_b \\ (\lambda_{kj}^{(n)} + \lambda_{jk}^{(n)}) \mathbf{J}_r(\phi_{kj}^{(n)}), & j \in \mathcal{N}_a \end{cases} \quad (66)$$

and in (64b), $\mathbf{T}^{(n)} \in \mathbb{S}_{++}^{2N_a}$ is given by $\mathbf{T}^{(n)} = \sum_{k \in \mathcal{N}_a} \mathbf{E}_{k,k}^{N_a} \otimes \mathbf{T}_k^{(n)}$ with $\mathbf{T}_k^{(n)} = \lambda_{kk}^{(n)} \mathbf{I}_2$.

Remark 6: Theorem 4 shows that the EFIM for the positions can be decomposed into two parts, i.e., the information corresponding to spatial cooperation and temporal cooperation, respectively, represented by $\mathbf{J}_e^s(\mathbf{p})$ and $\mathbf{J}_e^t(\mathbf{p})$. Each part can be further decomposed into basic building blocks $\mathbf{S}_{kj}^{(n)}$ and $\mathbf{T}_k^{(n)}$ with a structure detailed in the following.

- The contribution from spatial cooperation $\mathbf{J}_e^s(\mathbf{p})$ characterizes the location information obtained from the inter-node measurements among the agents at each instant. It is a block-diagonal matrix with each block $\mathbf{S}^{(n)}$ of size $2N_a \times 2N_a$ structured as in (65), characterizing the information of the inter-node measurements at time t_n . In particular, the rank-1 submatrix $\mathbf{S}_{kj}^{(n)}$ denotes the RI obtained from the inter-node measurement between nodes k and j at time t_n ; the k th-diagonal block of $\mathbf{S}^{(n)}$ is the summation of the RI between agent k and all other nodes, while the offdiagonal blocks are the negation of the RI between each pair of agents.
- The contribution from temporal cooperation $\mathbf{J}_e^t(\mathbf{p})$ characterizes the location information obtained from the intra-node measurements of each agent. It has a diagonally striped structure with each block $\mathbf{T}^{(n)}$ of size $2N_a \times 2N_a$, characterizing the information of the intra-node measurements from time t_n to t_{n+1} . The matrix $\mathbf{T}^{(n)}$ is block-diagonal with each block being a 2×2 matrix corresponding to

$\mathbf{p}_k^{(n)}$'s, since the intranode measurements of different agents are independent. Moreover, those $\mathbf{T}^{(n)}$ on the off-diagonal of $\mathbf{J}_e^t(\mathbf{p})$ is due to the fact that the intra-node measurements are related to the agent positions at two consecutive instants according to (15). Note also that the displacement model (15) for intra-node measurements simplifies each building block to $\mathbf{T}_k^{(n)} = \sigma_m^{-2} \mathbf{I}_2$. However, in general, $\mathbf{T}_k^{(n)}$ can be any 2×2 positive-semidefinite matrix depending on the type of intra-node measurements, which can be composed of the range and direction component.

In the Bayesian case, when prior knowledge of the agent positions and their dynamic models is available, there will be an additional component $\mathbf{J}_p(\mathbf{p})$ in (63), similar to that in (61). This component characterizes the contribution of the prior knowledge, and it has a structure similar to $\mathbf{J}_e^t(\mathbf{p})$ because the knowledge of agents' dynamic models accounts for the relationship of their positions at consecutive instants.

To better visualize the above results, consider a simple dynamic network example of three agents at two instants, i.e., $N_a = 3$ and $N = 2$, as illustrated in Fig. 4. In cooperative navigation, temporal cooperation gives another layer of information across consecutive instants, in addition to the spatial cooperation at each instant.

In most real-time applications, one may be only interested in the localization performance of the current time t_N , i.e., the EFIM $\mathbf{J}_e(\mathbf{p}^{(N)})$. It can be derived recursively based on the diagonally striped structure of the EFIM $\mathbf{J}_e(\mathbf{p})$ in (63). To enable the recursion, we define the notion of carry-over information from t_{n-1} to t_n as

$$\tilde{\mathbf{T}}^{(n)} := \mathbf{T}^{(n)} - \mathbf{T}^{(n)} \left(\mathbf{S}^{(n-1)} + \tilde{\mathbf{T}}^{(n-1)} + \mathbf{T}^{(n)} \right)^{-1} \mathbf{T}^{(n)} \quad (67)$$

with $\tilde{\mathbf{T}}^{(1)} := \mathbf{0}$. Based on the carry-over information, the EFIM for $\mathbf{p}^{(n:N)}$ can be written as

$$\begin{aligned} \mathbf{J}_e(\mathbf{p}^{(n:N)}) &= \mathbf{E}_{1,1}^{N-n+1} \otimes \left(\mathbf{S}^{(n)} + \tilde{\mathbf{T}}^{(n)} + \mathbf{T}^{(n+1)} \right) \\ &\quad + \sum_{m=n+1}^N \mathbf{E}_{m-n+1, m-n+1}^{N-n+1} \otimes \left(\mathbf{S}^{(m)} + \mathbf{T}^{(m)} + \mathbf{T}^{(m+1)} \right) \\ &\quad - \sum_{m=n+1}^N \left(\mathbf{E}_{m-n, m-n+1}^{N-n+1} + \mathbf{E}_{m-n+1, m-n}^{N-n+1} \right) \otimes \mathbf{T}^{(m)}. \end{aligned} \quad (68)$$

Comparison of (68) and the original EFIM (63) shows that the carry-over information $\tilde{\mathbf{T}}^{(n)}$ retains all the useful information at t_{n-1} for the EFIM $\mathbf{J}_e(\mathbf{p}^{(n:N)})$. Such information is transferred from one instant to the next through temporal cooperation. Based on (67), the carry-over information for cooperative navigation can be obtained

¹⁹For notational convenience, we let $\mathbf{T}^{(1)} = \mathbf{T}^{(N+1)} = \mathbf{0}$.

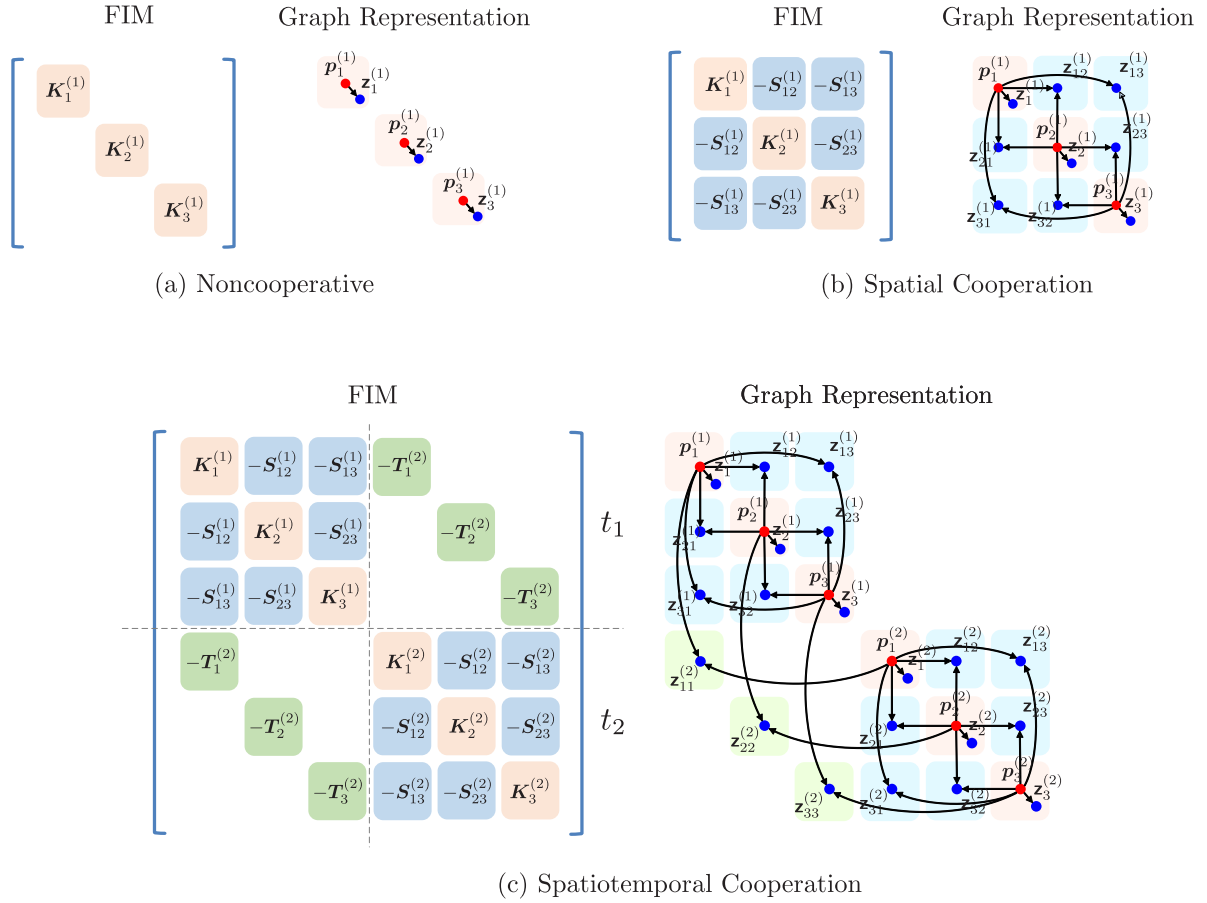


Fig. 4. FIM and the graphical representation of the states and measurements. (a) In scenarios without cooperation, the EFIM is block diagonal, and the graph of different agents are separated, i.e., $K_k^{(n)} = \sum_{j \in \mathcal{N}_b} S_{kj}^{(n)}$. (b) In scenarios with spatial cooperation, the EFIM has off-diagonal block that corresponds to the spatial cooperation measurements, and the graph has measurement nodes that connect different agents, i.e., $K_k^{(n)} = \sum_{j \in \mathcal{N}_a \cup \mathcal{N}_b \setminus \{k\}} S_{kj}^{(n)}$. (c) In scenarios with spatiotemporal cooperation, the EFIM further has off-diagonal blocks corresponding to temporal measurements, and the graph has measurement nodes that connect agents at consecutive time instants, i.e., $K_k^{(n)} = \sum_{j \in \mathcal{N}_a \cup \mathcal{N}_b \setminus \{k\}} S_{kj}^{(n)} + T_k^{(n)} + T_k^{(n+1)}$.

recursively at each instant and used as prior knowledge of the agent positions for the next instant. After $N - 1$ steps, we can obtain the EFIM $J_e(\mathbf{p}^{(N)})$.

Note that spatial cooperation generally results in coupled inference, illustrated by the non-block-diagonal structure of $S^{(n-1)}$ in (67) [55]. Thus, although $T^{(n)}$ is block-diagonal due to the independence of the intra-node measurements corresponding to different agents, the carry-over information $\tilde{T}^{(n)}$ has a complicated structure. In distributed networks, the agents usually do not capture the correlation of their location information arising from spatial cooperation, and only keep their individual (marginal) position distributions. Hence, we obtain an approximate EFIM by ignoring such correlation at each instant, which yields more insights into the entire navigation process.

For distributed networks, the exact individual EFIM for agent k at time t_{n-1} after spatial cooperation is given by

$$\tilde{S}_k^{(n-1)} = \left\{ \left[\left(S^{(n-1)} + \tilde{T}^{(n-1)} \right)^{-1} \right]_{\mathbf{p}_k^{(n-1)}} \right\}^{-1}. \quad (69)$$

Thus, by ignoring the correlation in carry-over information, the EFIM after spatial cooperation can be approximated

$$\tilde{S}^{(n-1)} \approx \sum_{k \in \mathcal{N}_a} \mathbf{E}_{k,k}^{N_a} \otimes \tilde{S}_k^{(n-1)} \quad (70)$$

and this leads to the approximate carry-over information (67) at time t_n

$$\tilde{T}^{(n)} \approx \sum_{k \in \mathcal{N}_a} \mathbf{E}_{k,k}^{N_a} \otimes \tilde{T}_k^{(n)} \quad (71)$$

where the individual carry-over information for agent k is

$$\tilde{T}_k^{(n)} = T_k^{(n)} - T_k^{(n)} \left(\tilde{S}_k^{(n-1)} + T_k^{(n)} \right)^{-1} T_k^{(n)}. \quad (72)$$

Note also that (67) reduces to (72) for the cases without spatial cooperation since the approximation (70) becomes exact.

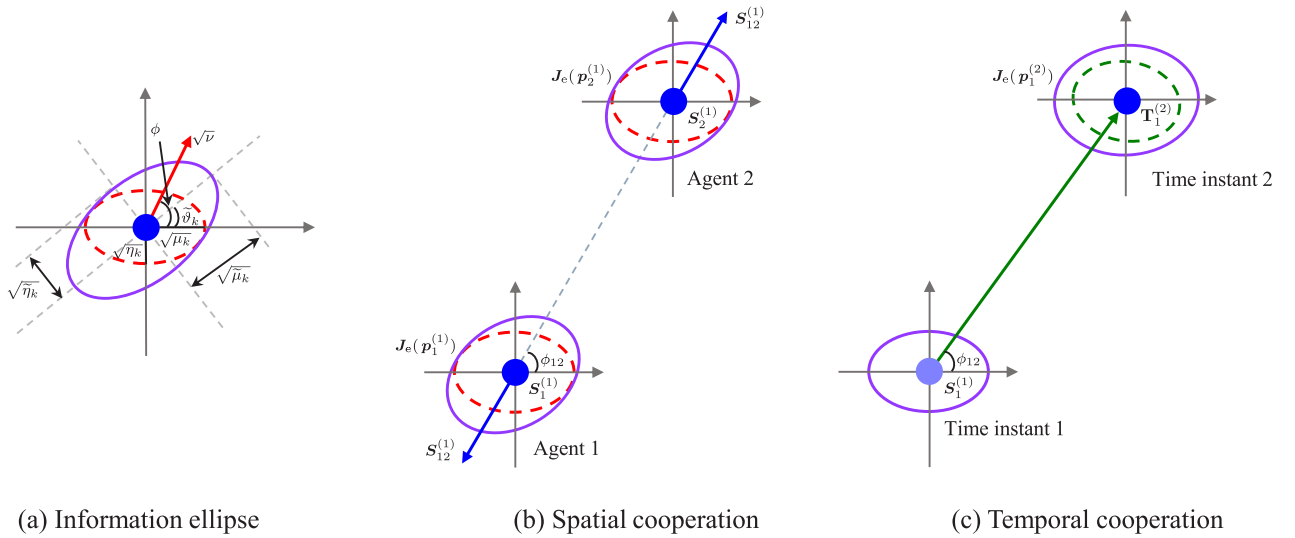


Fig. 5. Information ellipse and its evolution in the spatial and temporal domains. (a) The information ellipse with the length of major and minor axes given by $\sqrt{\mu_k}$ and $\sqrt{\eta_k}$, respectively. When another anchor is added, the major and minor axes of the ellipse grow to $\sqrt{\mu_k + \nu}$ and $\sqrt{\eta_k}$; (b) Spatial cooperation increases the ellipse along the line adjoining the two nodes; (c) Temporal cooperation increases the ellipse along two orthogonal directions, which are determined jointly by the intra-node measurement and the spatial information at the previous time instant.

By the approximation in (70), the location information evolution in cooperative navigation can be interpreted as follows: at each instant, the agents do the following:

- treat their own carry-over information as prior knowledge, and update their (marginal) position distribution using inter-node measurements with neighbors, as in the spatial step (69);
- obtain the carry-over information for the next instant based on their own position distribution and intranode measurements, as in the temporal step (72).

V. GEOMETRIC INTERPRETATION

This section presents a geometric interpretation of the EFIM for NLN, providing insights into the design and analysis of localization systems and algorithms. We begin with static networks without and with spatial cooperation, and then extend to the dynamic networks with spatiotemporal cooperation.

A. Information Ellipse

The EFIM for agent k 's position for noncooperative scenarios, given by (27), can be rewritten using eigenvalue decomposition as

$$\mathbf{J}_e(\mathbf{p}_k) = \mathbf{u}_{\vartheta_k} \begin{bmatrix} \mu_k & 0 \\ 0 & \eta_k \end{bmatrix} \mathbf{u}_{\vartheta_k}^T \quad (73)$$

where $\mu_k \geq \eta_k$ are the eigenvalues of $\mathbf{J}_e(\mathbf{p}_k)$ and \mathbf{u}_{ϑ_k} is a rotation matrix with angle ϑ_k , given by

$$\mathbf{u}_{\vartheta_k} = \begin{bmatrix} \cos \vartheta_k & -\sin \vartheta_k \\ \sin \vartheta_k & \cos \vartheta_k \end{bmatrix}. \quad (74)$$

The first and second columns of \mathbf{u}_{ϑ_k} are eigenvectors corresponding to eigenvalues μ_k and η_k , respectively. By the properties of eigenvalues, we have

$$\mu_k + \eta_k = \text{tr}\{\mathbf{J}_e(\mathbf{p}_k)\} = \sum_{j \in \mathcal{N}_b} \lambda_{kj} \quad (75)$$

and the SPEB for agent k given by

$$\mathcal{P}(\mathbf{p}_k) = \text{tr}\{\mathbf{J}_e^{-1}(\mathbf{p}_k)\} = \mu_k^{-1} + \eta_k^{-1}. \quad (76)$$

Definition 4 (Information Ellipse): The information ellipse of EFIM $\mathbf{J} \in \mathbb{S}_{++}^2$ is defined as the sets of points

$$\{\mathbf{w} \in \mathbb{R}^2 : \mathbf{w}^T \mathbf{J}^{-1} \mathbf{w} = 1\}. \quad (77)$$

Fig. 5 (a) depicts an information ellipse, which corresponds to an EFIM, with major and minor axes equal to $\sqrt{\mu_k}$ and $\sqrt{\eta_k}$, respectively, and a rotation ϑ_k from the reference coordinate. Moreover, the RI from a new anchor can be viewed as a degenerated information ellipse with the major axis equal to $\sqrt{\nu}$ and the minor axis equal to 0 with a rotation ϕ . The information ellipse of the new EFIM then grows along the direction ϕ .

Assuming $\vartheta_k = 0$ in (73), with the additional RI as shown in Fig. 5 (a), the new EFIM is represented by

$$\tilde{\mathbf{J}}_e(\mathbf{p}_k) = \begin{bmatrix} \mu_k & 0 \\ 0 & \eta_k \end{bmatrix} + \nu \mathbf{u}(\phi) \mathbf{u}(\phi)^T \quad (78)$$

which is equivalent to an information ellipse with the major, minor axes, and rotation angle given by

$$\tilde{\mu}_k, \tilde{\eta}_k = \frac{\mu_k + \eta_k + \nu}{2} \pm \frac{1}{2} \sqrt{[\mu_k - \eta_k + \nu \cos 2\phi]^2 + \nu^2 \sin^2 2\phi} \quad (79a)$$

$$\tilde{\vartheta}_k = \frac{1}{2} \arctan \left(\frac{\nu \sin 2\phi}{\mu_k - \eta_k + \nu \cos 2\phi} \right). \quad (79b)$$

The corresponding SPEB becomes

$$\tilde{\mathcal{P}}(\mathbf{p}_k) = \frac{1}{\tilde{\mu}_k} + \frac{1}{\tilde{\eta}_k} = \frac{\mu_k + \eta_k + \nu}{\mu_k \eta_k + \nu [\eta_k + (\mu_k - \eta_k) \sin^2 \phi]} \quad (80)$$

which is no greater than $\mathcal{P}(\mathbf{p}_k)$.

For a fixed RII ν , $\tilde{\mathcal{P}}(\mathbf{p}_k)$ in (80) can be minimized through ϕ in the denominator

$$\min_{\phi} \tilde{\mathcal{P}}(\mathbf{p}_k) = \frac{\mu_k + \eta_k + \nu}{\mu_k(\eta_k + \nu)} \quad (81)$$

with

$$\arg \min_{\phi} \tilde{\mathcal{P}}(\mathbf{p}_k) = \pm \pi/2. \quad (82)$$

That is, the additional anchor provides the largest reduction in terms of SPEB when it is along the direction of the eigenvector corresponding to the smaller eigenvalue η_k (or the least reduction when it is along the direction of the eigenvector corresponding to the larger eigenvalue μ_k). In other words, the minimum SPEB is achieved when the new anchor is placed along the minor axis of the information ellipse corresponding to $\mathbf{J}_e(\mathbf{p}_k)$ (or the maximum SPEB is achieved when the new anchor is along the major axis of the information ellipse). Moreover, the SPEB with the additional anchor can be bounded as

$$\mu_k^{-1} < \tilde{\mathcal{P}}(\mathbf{p}_k) \leq \mathcal{P}(\mathbf{p}_k) \quad (83)$$

where the lower and upper bounds are obtained by setting ν to $+\infty$ and 0, respectively

$$\mu_k^{-1} = \lim_{\nu \rightarrow +\infty} \tilde{\mathcal{P}}(\mathbf{p}_k)|_{\phi_k = \pm \pi/2} \quad (84a)$$

$$\mathcal{P}(\mathbf{p}_k) = \lim_{\nu \rightarrow 0} \tilde{\mathcal{P}}(\mathbf{p}_k). \quad (84b)$$

B. Information Ellipse for Spatial Cooperation

The EFIM for individual agents can be further obtained from the EFIM for spatial cooperation given in (56) by using the methodology of EFI. In general, the expression for the individual EFIM is complicated [55], but we can find its lower and upper bounds with simple expressions.

Based on the definitions of $\mathbf{J}_e^A(\mathbf{p}_k)$ and $\mathbf{S}_{k,j}$ given in Theorem 3, we can bound the individual EFIM for agent k as

$$\mathbf{J}_e^L(\mathbf{p}_k) \preceq \mathbf{J}_e(\mathbf{p}_k) \preceq \mathbf{J}_e^U(\mathbf{p}_k) \quad (85)$$

where

$$\mathbf{J}_e^L(\mathbf{p}_k) = \mathbf{J}_e^A(\mathbf{p}_k) + \sum_{j \in \mathcal{N}_a \setminus \{k\}} \frac{1}{1 + \lambda_{kj} \Delta_{kj}} \mathbf{S}_{k,j} \quad (86a)$$

$$\mathbf{J}_e^U(\mathbf{p}_k) = \mathbf{J}_e^A(\mathbf{p}_k) + \sum_{j \in \mathcal{N}_a \setminus \{k\}} \frac{1}{1 + \lambda_{kj} \tilde{\Delta}_{kj}} \mathbf{S}_{k,j} \quad (86b)$$

in which

$$\Delta_{kj} = \mathbf{u}^T(\phi_{kj}) \left[\mathbf{J}_e^A(\mathbf{p}_j) \right]^{-1} \mathbf{u}(\phi_{kj})$$

$$\tilde{\Delta}_{kj} = \mathbf{u}^T(\phi_{kj}) \left[\mathbf{J}_e^A(\mathbf{p}_j) + \sum_{k' \in \mathcal{N}_a \setminus \{k,j\}} 2 \mathbf{S}_{k',j} \right]^{-1} \mathbf{u}(\phi_{kj}).$$

The inequalities in (85) show that the bounds for the EFIM can be written as weighted sums of RI from the neighboring anchors and agents. In particular, those from anchors have weights equal to 1, whereas those from agents have weights between 0 and 1. Such a degradation is due to the position uncertainty of the neighboring agents. The weights and the RI in (86a) and (86b) can be determined using only local information of agent k , and hence these bounds can be used to guide the design and analysis of cooperative localization networks [130].

As a special case of only two agents in cooperation (i.e., agent 1 and agent 2), it turns out that the lower and upper bounds in (85) coincide, leading to the following exact expression for the individual EFIM:

$$\mathbf{J}_e(\mathbf{p}_1) = \mathbf{J}_e^A(\mathbf{p}_1) + \frac{1}{1 + \lambda_{12} \Delta_{12}} \mathbf{S}_{12} \quad (87)$$

where $\Delta_{12} = \mathbf{u}^T(\phi_{12}) \left[\mathbf{J}_e^A(\mathbf{p}_2) \right]^{-1} \mathbf{u}(\phi_{12})$. In addition, $\mathbf{J}_e(\mathbf{p}_2)$ has a symmetric expression to (87). The information ellipses before and after cooperation are depicted in Fig. 5, where the new information ellipse grows along the line connecting the two agents.

Due to the inherent uncertainty of agent 2's position, the *effective* RII that agent 2 provides to agent 1 in (87) is

$$\tilde{\lambda}_{12} = \frac{\lambda_{12}}{1 + \lambda_{12} \Delta_{12}} \quad (88)$$

which is degraded from the original RII λ_{12} unless $\Delta_{12} = 0$. That is, unlike that from anchors, agent 1 cannot fully utilize the RI from agent 2. Note that Δ_{12} can be viewed as a directional squared ranging error of agent 2, based purely on the anchor information $\mathbf{J}_e^A(\mathbf{p}_2)$ along angle ϕ_{12} between the two agents. This implies that the larger the uncertainty of agent 2 along the angle ϕ_{12} , the less

effective the cooperation is. For a given Δ_{12} , the effective RII $\tilde{\lambda}_{12}$ increases monotonically with λ_{12} , and has the asymptotic limits

$$\lim_{\lambda_{12} \rightarrow 0} \tilde{\lambda}_{12} = 0 \quad (89a)$$

$$\lim_{\lambda_{12} \rightarrow \infty} \tilde{\lambda}_{12} = \Delta_{12}^{-1}. \quad (89b)$$

Hence, the maximum effective RII that agent 2 can provide to agent 1 is limited by the inverse of the directional squared ranging error of agent 2 along the angle ϕ_{12} .

Note that there is no degradation of RII when $\Delta_{12} = 0$, which corresponds to the scenarios that agent 2 has no position uncertainty along the direction of ϕ_{12} . In this case, agent 2 can be thought of as an anchor in providing RI to agent 1.

C. Information Evolution in Spatiotemporal Cooperation

Finally, we provide a geometric interpretation for spatiotemporal cooperation to illustrate the information evolution of NLN. This section will focus on the carry-over information for distributed networks.

Recall that in the distributed settings, the EFIM (72) is a block-diagonal matrix with 2×2 blocks. We thus consider a single agent at one instant and simplify the notation of the carry-over information as

$$\tilde{T} = T - T(S + T)^{-1}T \quad (90)$$

where we decompose the spatial and temporal matrices as

$$S = \mu \mathbf{J}_r(\vartheta) + \eta \mathbf{J}_r(\vartheta + \pi/2) \quad (91a)$$

$$T = \zeta \mathbf{J}_r(\theta) + \xi \mathbf{J}_r(\theta + \pi/2) \quad (91b)$$

in which $\mu \geq \eta \geq 0$, $\zeta \geq \xi \geq 0$, and $\vartheta, \theta \in [0, \pi)$. For the ease of discussion, we denote $\mathbf{U} := \zeta \mathbf{J}_r(\theta)$ and $\mathbf{V} := \xi \mathbf{J}_r(\theta + \pi/2)$ as a decomposition of the temporal matrix.

The carry-over information in (90) can be rewritten, after some algebra, as

$$\tilde{T} = q_1 \mathbf{U} + q_2 \mathbf{V} + q_3 [\mathbf{J}_r(\theta + \pi/4) - \mathbf{J}_r(\theta - \pi/4)] \quad (92)$$

where the coefficients are given by

$$q_1 = [1 + \zeta \mathbf{u}^T(\theta)(S + V)^{-1} \mathbf{u}(\theta)]^{-1} \quad (93a)$$

$$q_2 = [1 + \xi \mathbf{u}^T(\theta + \pi/2)(S + U)^{-1} \mathbf{u}(\theta + \pi/2)]^{-1} \quad (93b)$$

$$q_3 = -\zeta \xi \mathbf{u}^T(\theta)(S + U + V)^{-1} \mathbf{u}(\theta + \pi/2). \quad (93c)$$

The expression (92) of the carry-over information can be represented as a sum of three terms: the first two terms represent two orthogonal components of the location information obtained from temporal cooperation, in which the

weights are between 0 and 1 depending on the directional position uncertainty of the agent after spatial cooperation, and the third term characterizes the coupling of the information between the spatial and temporal cooperation. For the coupling term, note that $\mathbf{J}_r(\theta + \pi/4) - \mathbf{J}_r(\theta - \pi/4)$ has the eigenvalues and eigenvectors $\{1, \mathbf{u}(\theta + \pi/4)\}$ and $\{-1, \mathbf{u}(\theta - \pi/4)\}$. Moreover, since the coefficient q_3 in (93c) can also be written as

$$q_3 = \frac{\zeta \xi (\mu - \eta) \sin(2(\vartheta - \theta))}{|S + U + V|} \quad (94)$$

the coupling term increases the EFIM with the intensity $|q_3|$ in the direction of $\theta + \pi/4$ and decreases with the same amount in the direction of $\theta - \pi/4$ if $\sin(2(\vartheta - \theta)) > 0$, and *vice versa* if $\sin(2(\vartheta - \theta)) < 0$. This intensity vanishes when 1) $\eta = \mu$; 2) $|\vartheta - \theta| = 0$ or $\pi/2$; or 3) $\xi = 0$. In the first two cases, the eigenvectors corresponding to T align with those of S , and

$$\tilde{T} = \begin{cases} \frac{\zeta \mu}{\zeta + \mu} \mathbf{J}_r(\theta) + \frac{\eta \xi}{\eta + \xi} \mathbf{J}_r(\theta + \pi/2), & |\vartheta - \theta| = 0 \\ \frac{\zeta \eta}{\zeta + \eta} \mathbf{J}_r(\theta + \pi/2) + \frac{\eta \xi}{\eta + \xi} \mathbf{J}_r(\theta), & |\vartheta - \theta| = \pi/2. \end{cases} \quad (95)$$

In the third case, the location information from temporal cooperation degenerates to a 1-D matrix. That is, $T = U$ and thus the carry-over information $\tilde{T} = q_1 U$ also degenerates to a 1-D matrix. Finally, as a geometric interpretation, temporal cooperation increases the information ellipse along two orthogonal directions, as depicted in Fig. 5(c).

In summary, the carry-over information \tilde{T} depends on both the location information after spatial cooperation at the previous instant and the information obtained from the intra-node measurements. Due to the position uncertainty characterized by the location information S , it can be shown that $\tilde{T} \preceq T$.

Leveraging the discussion for spatial and temporal cooperation, we illustrate the information evolution of NLN induced by spatiotemporal cooperation in Fig. 6. The three ellipses of each agent correspond to the initial carry-over information, the information after anchors' contribution, and the information after spatial cooperation, respectively.

VI. MAP INFORMATION AND ALGORITHM ASPECTS

In this section, we will discuss two important issues related to the theoretical foundation of NLN. First, we will quantify the benefit of map information, which can be treated as prior knowledge for localization, from a theoretical perspective. Second, we will present general forms for localization algorithms and the challenges in designing efficient distributed solutions.

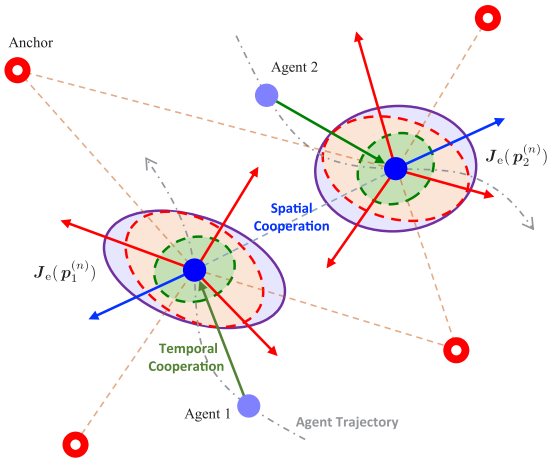


Fig. 6. Geometric interpretation of spatiotemporal cooperation. The green ellipse denotes the EFIM of each agent carried from time t_{n-1} to time t_n through temporal cooperation; the blue dashed ellipse denotes the EFIM after making inter-node measurement with anchors; and the orange ellipse denotes the EFIM at time t_n through spatial cooperation between the two agents.

A. Map-Aware Localization

While map information has been implicitly used in localization systems, there are only a few theoretical studies that analyze the benefit of map information. In particular, performance bounds have been derived to characterize the relationship between the localization accuracy and the map information for noncooperative localization in [89] and cooperative localization in [90]. We next outline a theoretical analysis of a map-aware localization network for both noncooperative and cooperative networks.

Suppose that agent k is placed in a 2-D area \mathcal{R} . Without additional knowledge, the prior pdf of its position $f(\mathbf{p}_k)$ is commonly modeled by a uniform distribution

$$f(\mathbf{p}_k) = \begin{cases} 1/|\mathcal{R}|, & \mathbf{p}_k \in \mathcal{R} \\ 0, & \text{elsewhere} \end{cases} \quad (96)$$

where $|\mathcal{R}|$ denotes the area of \mathcal{R} , as uniform distributions have the maximum entropy given a finite support.

For simplicity, we consider static scenarios and assume that the position measurement $\mathbf{z}_k \in \mathbb{R}^2$ of agent k based on the inter-node measurements from anchors follows a Gaussian distribution with mean \mathbf{p}_k and variance $\sigma_b^2 \mathbf{I}_2$, and the inter-node measurement \mathbf{z}_{kj} between agent k and agent j follows a Gaussian distribution with mean $\mathbf{p}_k - \mathbf{p}_j$ and variance $\sigma_a^2 \mathbf{I}_2$, where σ_b^2 and σ_a^2 are the error variances of the corresponding measurements.²⁰

The MSE matrix of the position estimation $\hat{\mathbf{p}}(\mathbf{z})$ based on the measurement \mathbf{z} is given by

$$\Lambda := \mathbb{E}_{\mathbf{z}, \mathbf{p}} \left\{ [\hat{\mathbf{p}}(\mathbf{z}) - \mathbf{p}] [\hat{\mathbf{p}}(\mathbf{z}) - \mathbf{p}]^T \right\} \quad (97)$$

²⁰While the simplest nontrivial models are adopted for ease of exposition, the analysis is applicable when the measurements are received waveforms or the measurement noise has a nondiagonal covariance matrix.

and the MSE for agent k 's position estimator in x and y coordinates can be written, respectively, as $\sigma_{k_x}^2 = [\Lambda]_{2k-1, 2k-1}$ and $\sigma_{k_y}^2 = [\Lambda]_{2k, 2k}$.

Attainable lower bounds on the MSE of the estimator are often employed to characterize the performance of the estimator. The most commonly used CRLB is not appropriate to evaluate the map-aware localization because the agent positions are modeled as RVs in (97) rather than the deterministic parameters. Moreover, simple extension of the CRLB to the Bayesian case still cannot fully capture the map information due to the violation of the regularity conditions. Therefore, we next present the ZZB and WWB, which adopt different ways to incorporate the map information, to characterize the localization performance.

1) *Ziv-Zakai Bound (ZZB)*: We first give a brief review of the ZZB in the context of NLN. The derivation of the ZZB relies on transforming the estimation error into a related hypothesis testing problem, and the bound is tightened by the optimal decision rule [145].

For any estimator $\hat{\mathbf{p}}(\mathbf{z})$ of the agent positions, the estimation error is $\boldsymbol{\varepsilon} = \hat{\mathbf{p}}(\mathbf{z}) - \mathbf{p}$ with the MSE matrix Λ given by (97). The ZZB is derived from the following identity of the projected MSE of Λ along a given direction $\mathbf{a} \in \mathbb{R}^{2N_a}$ [148]

$$\mathbf{a}^T \Lambda \mathbf{a} = \mathbb{E}_{\mathbf{z}, \mathbf{p}} \{ \mathbf{a}^T \boldsymbol{\varepsilon} \boldsymbol{\varepsilon}^T \mathbf{a} \} = \frac{1}{2} \int_0^\infty \mathbb{P} \{ |\mathbf{a}^T \boldsymbol{\varepsilon}| \geq \frac{h}{2} \} h \, dh. \quad (98)$$

For a given $h > 0$, let $\boldsymbol{\delta}$ be any vector in \mathbb{R}^{2N_a} such that $\mathbf{a}^T \boldsymbol{\delta} = h$. Then the probability $\mathbb{P} \{ |\mathbf{a}^T \boldsymbol{\varepsilon}| \geq \frac{h}{2} \}$ can be calculated using binary hypothesis testing problems between two fixed agent position vectors \mathbf{p} and $\mathbf{p} + \boldsymbol{\delta}$, given by

$$\begin{cases} H_0 : \mathbf{z} \sim f_{\mathbf{z}}(\mathbf{z}; \gamma = 0) \\ H_1 : \mathbf{z} \sim f_{\mathbf{z}}(\mathbf{z}; \gamma = 1) \end{cases} \quad (99)$$

where $\mathbf{z} = \mathbf{g}(\mathbf{p} + \gamma \boldsymbol{\delta}) + \mathbf{w}$ in which $\mathbf{g}(\cdot)$ denotes the measurement function of the agent positions and the \mathbf{w} is the observation noise vector. Based on the prior PDF $f_{\mathbf{p}}(\mathbf{p})$ of the agent positions, the prior probability of hypothesis H_0 is given by

$$\mathbb{P}\{\gamma = 0\} = \frac{f_{\mathbf{p}}(\mathbf{p})}{f_{\mathbf{p}}(\mathbf{p}) + f_{\mathbf{p}}(\mathbf{p} + \boldsymbol{\delta})}$$

and that for H_1 is given by $1 = \mathbb{P}\{\gamma = 0\}$.

Let $P(\mathbf{p}, \mathbf{p} + \boldsymbol{\delta})$ be the decision error probability of the following suboptimal decision rule for (99)

$$\mathbf{a}^T \hat{\mathbf{p}}(\mathbf{z}) \underset{\gamma=0}{\overset{\gamma=1}{\geq}} \mathbf{a}^T \mathbf{p} + \frac{h}{2} \quad (100)$$

and then it can be shown that

$$\begin{aligned} & \mathbb{P}\left\{|\mathbf{a}^T \boldsymbol{\epsilon}| \geq \frac{h}{2}\right\} \\ &= \int_{\mathbb{R}^{2N_a}} [f_{\mathbf{p}}(\mathbf{p}) + f_{\mathbf{p}}(\mathbf{p} + \boldsymbol{\delta})] P(\mathbf{p}, \mathbf{p} + \boldsymbol{\delta}) d\mathbf{p}. \end{aligned} \quad (101)$$

Since $P(\mathbf{p}, \mathbf{p} + \boldsymbol{\delta})$ is lower bounded by the minimum error probability $P_{\min}(\mathbf{p}, \mathbf{p} + \boldsymbol{\delta})$ corresponding to the best rule for deciding H_0 and H_1 , the projected MSE in (98) is larger than or equal to the ZZB, given as follows

$$\begin{aligned} \mathbf{a}^T \boldsymbol{\Lambda} \mathbf{a} \geq & \frac{1}{2} \int_0^\infty \mathcal{V}\left\{ \max_{\boldsymbol{\delta}: \mathbf{a}^T \boldsymbol{\delta} = h} \left[\int_{\mathbb{R}^{2N_a}} (f_{\mathbf{p}}(\mathbf{p}) + f_{\mathbf{p}}(\mathbf{p} + \boldsymbol{\delta})) \right. \right. \\ & \left. \left. \cdot P_{\min}(\mathbf{p}, \mathbf{p} + \boldsymbol{\delta}) d\mathbf{p} \right] \right\} h dh \end{aligned} \quad (102)$$

where $\mathcal{V}(\cdot)$ is the ‘‘valley-filling’’ function to obtain a tighter bound using the non-increasing property of (101) with respect to h [148]. Since the distribution of the agent positions appears in the integral of (102), the ZZB naturally incorporates the prior map information in the mapaware NLN.

In the NLN problem, we consider the problem of estimating the position vector \mathbf{p}_k of agent k in the x -axis as an example, and the result for the y -axis follows from the same derivation. The MSE of the agent k 's position in the x -axis is bounded below by the ZZB as [90]

$$\sigma_{k_x}^2 \geq Z_{k_x} \quad (103)$$

where

$$\begin{aligned} Z_{k_x} := & \frac{1}{|\mathcal{R}|^{N_a}} \int_{\mathcal{Y}} \int_0^\infty \max_{\boldsymbol{\delta}_x: \mathbf{e}_{k, N_a}^T \boldsymbol{\delta}_x = h} \left\{ \int_{S(\boldsymbol{\rho}_y, \boldsymbol{\delta}_x)} \right. \\ & \left. Q(d_0(\boldsymbol{\delta}_x)/2) d\boldsymbol{\rho}_x \right\} h dh d\boldsymbol{\rho}_y \end{aligned} \quad (104)$$

in which $\boldsymbol{\rho}_x$ and $\boldsymbol{\rho}_y$ correspond to the x - and y -coordinates of vector $\boldsymbol{\rho}$ (so are $\boldsymbol{\delta}_x$ and $\boldsymbol{\delta}_y$ of vector $\boldsymbol{\delta}$), respectively

$$S(\boldsymbol{\rho}_y, \boldsymbol{\delta}_x) = \{\boldsymbol{\rho}_x | f(\boldsymbol{\rho}) > 0 \text{ and } f(\boldsymbol{\rho} + \boldsymbol{\delta}) > 0 \text{ and } \boldsymbol{\delta}_y = \mathbf{0}\}$$

\mathcal{Y} is the support of the y -coordinates of the vector \mathbf{p} given by (96), and $Q(\cdot)$ is the tail probability of the standard normal distribution. In (104), $d_0(\boldsymbol{\delta}_x)$ denotes the normalized distance in the x -axis between the means of the two likelihood functions in the hypothesis testing problem (99), and it is given by

$$d_0(\boldsymbol{\delta}_x) = \begin{cases} \|\boldsymbol{\delta}_x\|/\sigma_b, & \text{noncooperative} \\ \left(\frac{\|\boldsymbol{\delta}_x\|^2}{\sigma_b^2} + \sum_{k=1}^{N_a-1} \sum_{j=k+1}^{N_a} \frac{(\delta_{k_x} - \delta_{j_x})^2}{\sigma_a^2} \right)^{\frac{1}{2}}, & \text{cooperative} \end{cases} \quad (105)$$

where δ_{k_x} denotes the element of $\boldsymbol{\delta}$ corresponding to the x -axis of agent k . Based on (105), we can observe that cooperative localization can yield a smaller ZZB than noncooperative localization. This is due to the fact that $d_0(\boldsymbol{\delta}_x)$ in the cooperative case is larger than that in the noncooperative case and $Q(\cdot)$ is a monotonically decreasing function.

The ZZB presents a bound on the global MSE averaged over the prior PDF [148]. Compared with the CRLB, the ZZB is tighter in the entire SNR regions and has no restrictions on the type of the estimator. This provides a better performance benchmark to evaluate the achievable MSE. However, in most cases the maximization operator in (102) complicates the derivation of the ZZB in a closed form. Therefore, while the ZZB is a tighter bound than CRLB in the context of localization with prior knowledge, it is difficult to evaluate analytically.

2) *Weiss–Weistein Bound (WWB)*: We next present another type of bound that incorporates the prior knowledge in parameter estimation. Define $\psi(\mathbf{x}, \boldsymbol{\theta})$ for $\mathbf{x} \in \Omega$, $\boldsymbol{\theta} \in \Theta$ as a real-valued measurable function that satisfies the following condition [149]:

$$\int_{\Theta} \psi(\mathbf{x}, \boldsymbol{\theta}) f(\mathbf{x}, \boldsymbol{\theta}) d\boldsymbol{\theta} = 0, \quad \text{a.e. } \mathbf{x} \in \Omega \quad (106)$$

with $f(\mathbf{x}, \boldsymbol{\theta})$ being the joint pdf of \mathbf{x} and $\boldsymbol{\theta}$. Then, the following inequality holds for any real-valued scalar $k > 1$:

$$\mathbb{E}\{|g(\mathbf{x}) - h(\boldsymbol{\theta})|^k\} \geq \frac{|\mathbb{E}\{h(\boldsymbol{\theta})\psi(\mathbf{x}, \boldsymbol{\theta})\}|^k}{\left[\mathbb{E}\{|\psi(\mathbf{x}, \boldsymbol{\theta})|^{\frac{k}{k-1}}\}\right]^{k-1}} \quad (107)$$

where $g(\cdot)$ and $h(\cdot)$ are real-valued measurable functions defined on Ω and Θ , respectively.

In general, (107) represents a class of lower bounds for the estimation error of $h(\boldsymbol{\theta})$. As a special case with 1-D parameter θ and $k = 2$, the left-hand side becomes the common MSE for the estimator $g(\mathbf{x})$ of $h(\theta)$. If we take $h(\theta) = \theta$ and $\psi(\mathbf{x}, \theta)$ be the first partial derivative of $\ln f(\mathbf{x}, \theta)$ with respect to θ , then the above inequality reduces to exactly the CRLB.

To obtain the WWB for map-aware localization, we define

$$\begin{aligned} \psi(\mathbf{z}, \mathbf{p}) &= \begin{cases} L^\varsigma(\mathbf{z}; \mathbf{p} + \boldsymbol{\delta}, \mathbf{p}) - L^{1-\varsigma}(\mathbf{z}; \mathbf{p} - \boldsymbol{\delta}, \mathbf{p}), & \mathbf{p} \in S(\boldsymbol{\delta}) \\ 0, & \mathbf{p} \notin S(\boldsymbol{\delta}) \end{cases} \end{aligned} \quad (108)$$

where $S(\boldsymbol{\delta}) = \{\boldsymbol{\rho} | f(\boldsymbol{\rho}) > 0 \text{ and } f(\boldsymbol{\rho} + \boldsymbol{\delta}) > 0\}$, ς is a parameter between 0 and 1, and $L(\mathbf{z}; \mathbf{p}_1, \mathbf{p}_2) := f(\mathbf{z}, \mathbf{p}_1)/f(\mathbf{z}, \mathbf{p}_2)$.

One can easily verify that this definition of $\psi(\mathbf{z}, \mathbf{p})$ satisfies the requirement in (106). Again taking x -axis as

an example, we can derive the WWB for agent k in the cooperative localization as

$$\begin{aligned} \sigma_{k_x}^2 &\geq W_{k_x} \\ &:= \sup_{\delta \in \mathbb{R}^{2N_a}} \frac{(\delta_{k_x} \mathbb{E}_{\mathbf{z}, \mathbf{p}} \{L^\varsigma(\mathbf{z}; \mathbf{p}^+, \mathbf{p})\})^2}{\mathbb{E}_{\mathbf{z}, \mathbf{p}} \{ [L^\varsigma(\mathbf{z}; \mathbf{p}^+, \mathbf{p}) - L^\varsigma(\mathbf{z}; \mathbf{p}^-, \mathbf{p})]^2 \}} \end{aligned} \quad (109)$$

where $\mathbf{p}^+ := \mathbf{p} + \delta$ and $\mathbf{p}^- := \mathbf{p} - \delta$.

Note that unlike the CRLB, the derivation of the WWB is free of regularity conditions and thus the prior map information in terms of a uniform distribution can be easily incorporated in the bound. Indeed, since δ_{k_x} is a free variable and the CRLB is a special case in the limit $\delta_{k_x} \rightarrow 0$, the WWB that maximizes the right-hand side over all possible δ_{k_x} can be much tighter than the CRLB.

To simplify the exposition, we choose $\varsigma = \frac{1}{2}$ and the WWB can be further simplified into

$$W_{k_x} = \frac{1}{2|\mathcal{R}|^{N_a}} \sup_{\delta \in \mathbb{R}^{2N_a}} \frac{\left(\delta_{k_x} \int_{\mathcal{S}(\delta)} \exp(-d^2(\delta)/8) d\rho \right)^2}{\int_{\mathcal{S}(\delta)} d\rho - \int_{\tilde{\mathcal{S}}(\delta)} \exp(-d^2(\delta)/2) d\rho} \quad (110)$$

where

$$\tilde{\mathcal{S}}(\delta) := \{ \rho | f(\rho) > 0 \text{ and } f(\rho + \delta) > 0 \text{ and } f(\rho - \delta) > 0 \}$$

and

$$d(\delta) = \sqrt{d_0^2(\delta_x) + d_0^2(\delta_y)} \quad (111)$$

in which $d_0(\cdot)$ is defined in (105). The supremum operator leads to intractable expressions for the WWB, which hinders further investigation of the relationship between the map information and the localization accuracy. Nevertheless, the WWB tends to be tighter than the ZZB in certain SNR regions as shown in Fig. 7.

Numerical results are presented for a 1-D scenario in which three agents and two anchors are placed in a segment of length 10 m with the LOS measurements. The ratio of agent-agent measurement and agent-anchor measurement error variances σ_a^2/σ_b^2 is 1/200, i.e., cooperative internode measurements are of high quality. Fig. 7 compares the ZZB and WWB with the simulation results of the minimum mean squared error (MMSE) estimator. First, since the ZZB and WWB are tight over all SNR regimes, they can serve as good performance benchmarks for the achievable root mean squared error (RMSE) of map-aware localization.²¹ Moreover, the localization accuracy

²¹Unlike the RMSE obtained by the estimator, the calculation of ZZB and WWB does not require time-consuming simulations.

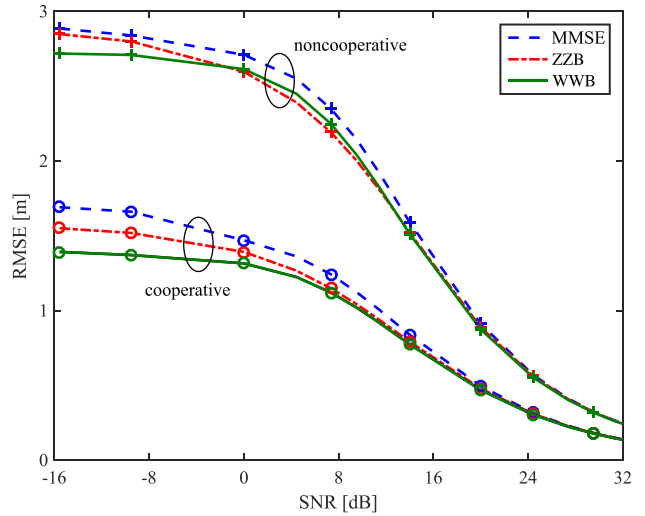


Fig. 7. RMSE as a function of the SNR of inter-node measurements with fixed ratio σ_a^2/σ_b^2 . The MMSE estimator, ZZB, and WWB are considered.

is considerably improved in the cooperation scenario in terms of the ZZB and WWB. Note that in the vicinity of low SNR regimes, the RMSE decreases slowly with the SNR, but there is a significant gain from cooperation due to high cooperation quality. Finally, in high SNR regimes, the measurements from anchors provide sufficient information, and hence the performance gap between cooperation and noncooperation is reduced.

B. Algorithm Design

The EFIM not only serves as a benchmark for practical NLN systems, but also provides important insights into how the system parameters and network geometry affect the localization performance. These insights will facilitate the algorithm design and system operation for efficient NLN.

Armed with the theoretical framework, we next present general forms for NLN algorithms, i.e., determining the agent states from inter-node and intra-node measurements. From a non-Bayesian perspective, the optimal algorithm amounts to determining the likelihood function $f(\mathbf{z}; \mathbf{p})$, from which the maximum-likelihood (ML) estimate can be obtained; whereas from a Bayesian perspective, it amounts to determining the posterior distribution $f(\mathbf{p}|\mathbf{z})$, also referred to as the position belief. Once this belief is obtained, point estimates can be obtained by computing the mean or mode, leading to the or maximum a posteriori (MAP) estimates, respectively.

In the following discussion, we will focus on the non-Bayesian perspective and adopt Gaussian distributions for the inter-node and intra-node measurement errors as an example. All the discussions also apply to the Bayesian perspective and general measurement models, where the design of localization algorithms needs to incorporate prior information and the specific error distributions.

No cooperation: In the static case, each agent individually determines its position using the measurements obtained only from anchors [see Fig. 4(a)]. For Gaussian ranging error models, the estimate for agent k 's position \mathbf{p}_k is the solution of the weighted least squares problem

$$\hat{\mathbf{p}}_{k, \text{ML}} = \arg \min_{\mathbf{p}_k} \sum_{j \in \mathcal{N}_b} \frac{1}{\sigma_{z_{kj}}^2} (z_{kj} - \|\mathbf{p}_k - \mathbf{p}_j\|)^2 \quad (112)$$

where $\sigma_{z_{kj}}^2$ is the error variance in the inter-node measurement z_{kj} . The EFIM for the agent positions and the graphical representation of the states and measurements are given side by side in Fig. 4(a). Since there are no inter-node measurements between the agents, the EFIM is block-diagonal and the graph has separate subnetworks, each corresponding to a single agent.

Spatial cooperation: When spatial cooperation among agents is available, the agents can refine their position estimate by incorporating the inter-node measurements with the position estimates of their neighbors. Fig. 4(b) shows the EFIM and the graph for the case of spatial cooperation. Again when the measurement errors follow Gaussian distributions, the estimate for all agent positions $\mathbf{p} = \mathbf{p}_{1:N_a}$ is the solution of the weighted least squares problem

$$\begin{aligned} \hat{\mathbf{p}}_{\text{ML}} = \arg \min_{\mathbf{p}} & \sum_{k \in \mathcal{N}_a} \sum_{j \in \mathcal{N}_b} \frac{1}{\sigma_{z_{kj}}^2} (z_{kj} - \|\mathbf{p}_k - \mathbf{p}_j\|)^2 \\ & + \sum_{k \in \mathcal{N}_a} \sum_{j \in \mathcal{N}_a \setminus \{k\}} \frac{1}{\sigma_{z_{kj}}^2} (z_{kj} - \|\mathbf{p}_k - \mathbf{p}_j\|)^2. \end{aligned} \quad (113)$$

Due to the inter-node measurements between the agents, the EFIM is no longer block-diagonal and the graph is connected, where both the off-block-diagonal submatrices and the links connecting different agent positions correspond to the inter-node measurements among agents.

Spatiotemporal cooperation: Finally, when the temporal cooperation is further incorporated, agents can jointly estimate their positions at a sequence of instants, i.e., $\mathbf{p} = \mathbf{p}_{1:N_a}^{(1:N)}$ using all the inter-node and intra-node measurements. When all the measurement errors follow Gaussian distributions, the estimate for \mathbf{p} is the solution of

$$\begin{aligned} \hat{\mathbf{p}}_{\text{ML}} & = \arg \min_{\mathbf{p}} \sum_{n=1}^N \sum_{k \in \mathcal{N}_a} \sum_{j \in \mathcal{N}_b} \frac{1}{\sigma_{z_{kj}}^{(n)}} (z_{kj}^{(n)} - \|\mathbf{p}_k^{(n)} - \mathbf{p}_j^{(n)}\|)^2 \\ & + \sum_{n=1}^N \sum_{k \in \mathcal{N}_a} \sum_{j \in \mathcal{N}_a \setminus \{k\}} \frac{1}{\sigma_{z_{kj}}^{(n)}} (z_{kj}^{(n)} - \|\mathbf{p}_k^{(n)} - \mathbf{p}_j^{(n)}\|)^2 \\ & + \sum_{n=1}^{N-1} \sum_{k \in \mathcal{N}_a} \frac{1}{\sigma_{z_{kk}}^{(n)}} (z_{kk}^{(n)} - \|\mathbf{p}_k^{(n)} - \mathbf{p}_k^{(n-1)}\|)^2 \end{aligned} \quad (114)$$

where the three components correspond to the measurements from anchors, spatial cooperation, and temporal cooperation, respectively. Due to the intra-node measurements of each agent, the addition of the temporal cooperation further increases the size of the EFIM and the graph, as shown in Fig. 4(c). The off-diagonal blocks in the EFIM across different instants account for the intra-node measurements, which also result in the links connecting agent positions at different instants in the graph.

In the above setting, the ranging errors are modeled as a Gaussian distribution. When they follow non-Gaussian distributions, the optimization process required for estimation can be computationally challenging, in which case (112)–(114) can be used as tractable suboptimal solutions. Moreover, a centralized processor is required for computing the estimate for all agents at all instants. Such a process is highly complex and inefficient especially in medium- to large-scale networks, because joint estimation requires high-dimensional inference and incurs large communication overhead [165]–[167]. For practical implementation, distributed algorithms for NLN are attractive, where the agent positions can be estimated and refined locally through iterative algorithms in the network. However, in the spatiotemporal cooperative setting, the optimal estimates of agent positions are correlated. This can be seen from the nondiagonal structure of the EFIM as well as the presence of cycles in the graph. Distributed algorithms usually ignore such correlation for simple implementation, which often results in suboptimal solutions. It is thus desirable to analyze the spatial and temporal coupling of the location information and develop algorithms that can better handle the tradeoff between performance and complexity in algorithm design [168].

VII. DESIGN GUIDELINES FOR NLN

This section illustrates the theoretical results obtained in previous sections with practical network settings and signal parameters. These numerical results shed light into how different system parameters affect the localization performance, thus serving as performance benchmarks and design guidelines for practical localization networks.

In this section, we consider a network with 36 anchors deployed on a regular 6×6 lattice with 100-m separation between two neighboring anchors, i.e., the convex hull of these anchors is a square area of 500 m by 500 m. The agents are randomly deployed in this area. The orthogonal frequency division multiplexing (OFDM) signals with the carrier frequency of $f_c = 2$ or 5 GHz, the bandwidth ranging from 2 to 20 MHz, and the subcarrier spacing of 15 kHz are used for range measurements. The number of subcarriers is determined by the total bandwidth divided by the subcarrier spacing. Unless otherwise specified, the power of the transmitting signal at each node is 1mW with a duration of 66.67 μs [169] and the noise figure is set to 5 dB.

The RIIs between anchors and agents are determined as follows: first, the LOS/NLOS states of anchor k to all agents are generated for the Urban Micro scenario [170],

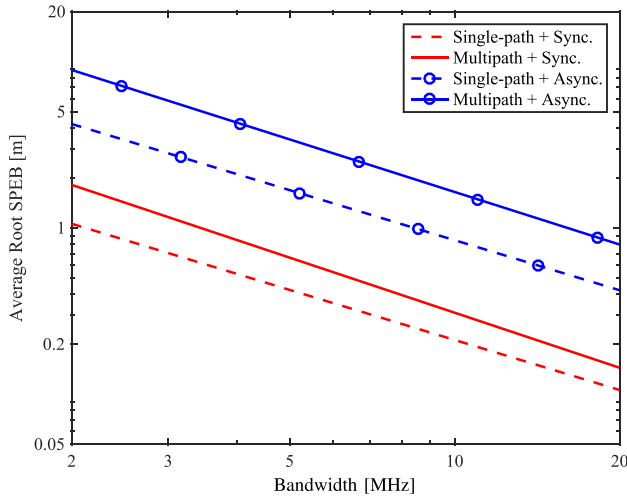


Fig. 8. Average root SPEB as a function of the signal bandwidth. The carrier frequency is 2 GHz. Both single-path and multipath channels as well as synchronous and asynchronous scenarios are considered.

with spatial consistency among agents according to [171]; then delays and amplitudes are generated using QuaDRiGa [172] according to the Urban Micro B1 for channels between anchor k and the agents with LOS states, where anchor k serves as the transmitter and the agents as the receivers; finally, the RIIs between anchor k and the agents with LOS states are then calculated based on [5], whereas those between anchor k and the agents with NLOS states are set to 0 [5]. The approach above considers the spatial consistency of channel fading from a particular anchor to several agents. Similarly, the RIIs among agents are determined by first generating LOS/ NLOS states as well as the delay and amplitudes, and then performing the calculation of the RII [54].

A. Signal and Channel Parameters

We first investigate the effect of various signal and channel parameters (e.g., signal bandwidth, multipath propagation, and clock biases) on the localization accuracy.²² One agent is randomly placed in the considered area, and the carrier frequency of the signal is 2 GHz. The localization accuracy of the agent is characterized by the root SPEB given in (27) and (38). Fig. 8 depicts the average root SPEB as a function of the signal bandwidth for both synchronous and asynchronous networks, where the averaging is over random node positions and channels. We draw the following observations from the figure.

The root SPEB decreases with the signal bandwidth, since the RII is proportional to the square of the effective

²²This paper focuses on fundamental limits of localization accuracy based on the RF signals. Practical imperfections in transceivers such as antenna radiation pattern, circuit implementation, and oscillator instability would degrade the localization accuracy with respect to that presented in this paper.

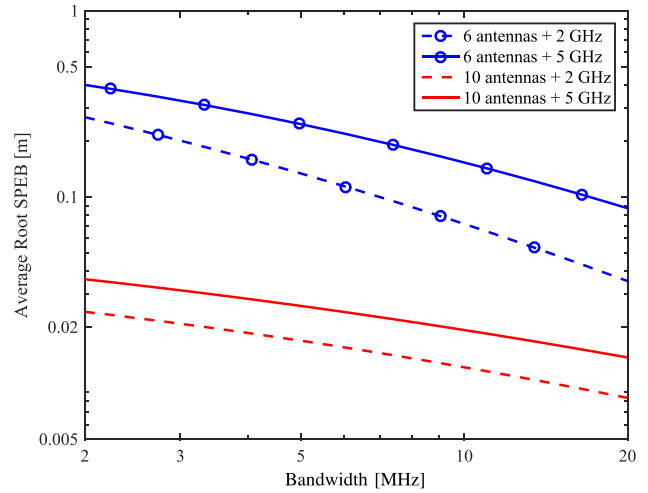


Fig. 9. Average root SPEB as a function of the signal bandwidth for localization with uniform linear arrays. Antenna arrays are of six or ten elements with interelement spacing 0.5 m, and multipath channels are considered.

bandwidth, as shown in (28). Indeed, in the log scale, one can verify from the figure that the root SPEB decreases linearly with the signal bandwidth, which is proportional to the effective bandwidth, with slope -1 for single-path channels. Moreover, in multipath channels, the root SPEB decreases faster with the signal bandwidth than that in single-path cases, i.e., the slopes of the corresponding curves are slightly smaller than -1 . This is because larger signal bandwidths give better channel resolvability, i.e., smaller path overlapping coefficient χ_{1j} in (31), which gives another fold of accuracy improvement. Nevertheless, the path overlapping effect itself causes larger root SPEB in multipath cases than single-path cases, due to the reduction of the RII by a factor $1 - \chi_{1j}$ in (31), whereas the gap in terms of the ratios between them decreases with the bandwidth, since larger bandwidth can reduce the effect of path overlapping.

We also compare the root SPEBs for asynchronous networks with those for synchronous networks. For both single-path and multipath cases, the root SPEBs as a function of the bandwidth for asynchronous networks behave similarly to those for the synchronous networks. Under the same network conditions, asynchronous networks have a poorer localization performance than the synchronous networks. This agrees with the theoretical results (38), as the unknown clock biases act as nuisance parameters in the inference problem. For example, in the multipath cases with signal bandwidth of 10 MHz, the root SPEBs are 0.31 and 1.64 m for synchronous and asynchronous networks, respectively. In fact, the ratios between the root SPEBs for synchronous and asynchronous cases are approximately constant for different bandwidths, as the ratio mainly depends on the network geometry rather than the signals and channels.

In summary, the figures in this section provide numerical examples of the theoretical results obtained in Section III,

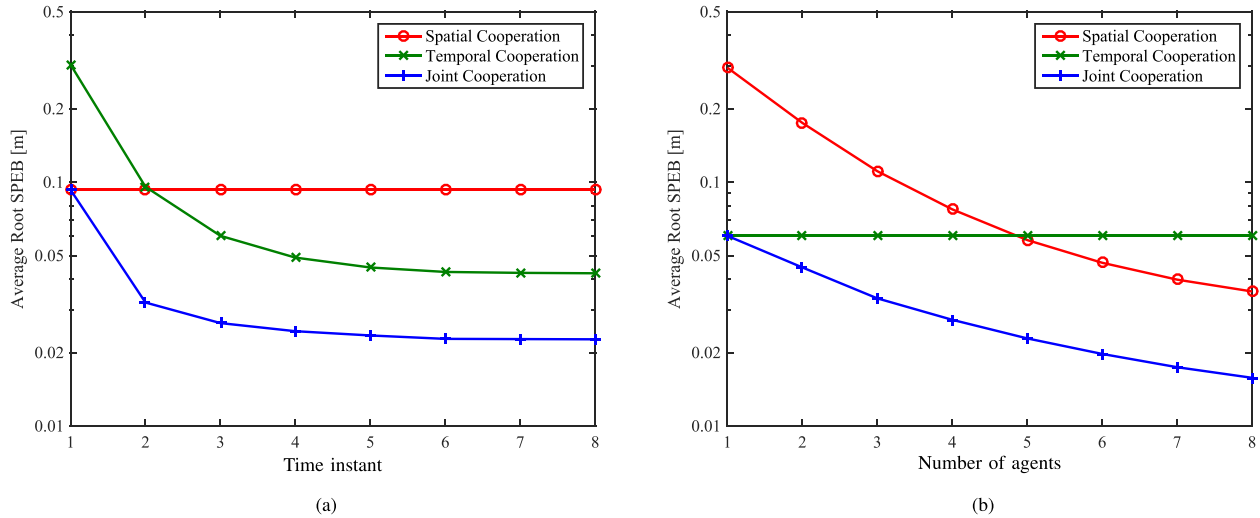


Fig. 10. Average root SPEB in cooperative networks as a function of (a) the instants with four agents and (b) the number of agents at the third instant. Three modes of cooperation are compared: spatial cooperation, temporal cooperation, and spatiotemporal cooperation.

quantifying the localization accuracy achieved by standard OFDM signals under realistic channel conditions. These results show how the signal bandwidth, multipath conditions, and clock biases affect the localization accuracy in practical systems.

B. Antenna Array Localization

We next investigate the performance of wireless localization systems where the anchors are equipped with antenna arrays. We adopt typical uniform linear arrays, where six or ten antenna elements are used. The carrier frequency of the signal is 2 or 5 GHz, and again one agent is randomly placed in the area. The localization accuracy of the agent is characterized by the root SPEB given in (52). Fig. 9 depicts the average root SPEB as a function of the signal bandwidth.

Compared with single-antenna systems in Fig. 8, antenna arrays significantly reduce the root SPEB. For example, for the OFDM signal with 2-MHz bandwidth and 2-GHz carrier frequency, localization using a six-antenna array yields an average root SPEB of 0.29 m, as opposed to 1.82 m using a single antenna, i.e., an approximately 85% reduction is achieved; for the signal with 10-MHz bandwidth and 2-GHz carrier frequency, the corresponding root SPEBs are 0.067 and 0.31 m for the six-antenna array and the single antenna, respectively, i.e., yielding an approximately 80% error reduction. Such performance gain is due to higher received SNR and additional angle information provided by the antenna array. As shown in Theorem 2, the AOA measurements can be obtained from the carrier phases of the received signals with an accuracy proportional to the carrier frequency, which is on the order of gigahertz. In contrast, the accuracy of the TOA measurements is proportional to the effective bandwidth of the baseband signal, which is on the order of megahertz. Thus, the performance gain using antenna

arrays is more remarkable when the bandwidth of the signals is an order of magnitudes smaller than the carrier frequency.

Note that for a given size of antenna arrays, the localization performance with carrier frequency 2 GHz is better than that with 5 GHz, which is counterintuitive. The explanation is as follows: although the accuracy of AOA measurements is proportional to the carrier frequency, the accuracy is also proportional to the received signal energy. A larger carrier frequency suffers from a more severe path loss, which reduces the SNR of received signals SNR_{1j} and thus the RII as shown in (53a)–(53b). Moreover, the ratio of the average root SPEBs for carrier frequency 5 GHz to those for 2 GHz increases with the bandwidth, which implies that the TOA measurements plays a more significant role in the localization information for the latter case. This is because the AOA measurements contribute more significantly to the overall localization information when the carrier frequency is 5 GHz more than when it is 2 GHz.

In addition, arrays with more antennas yield a better localization performance as expected. The gain is two-fold: one is the power gain as more received signal energy is collected at antennas, the other is the aperture gain as more antennas increase the array size, which yields better AOA estimation.

In summary, while more receive antennas always provide better localization performance, this set of results reveal the intricate roles of the carrier frequency and signal bandwidth on the localization accuracy. Hence, these signal parameters should be chosen carefully in practical antenna array localization systems.

C. Effects of Cooperation

We next investigate the localization performance with spatiotemporal cooperation. The network consists of the

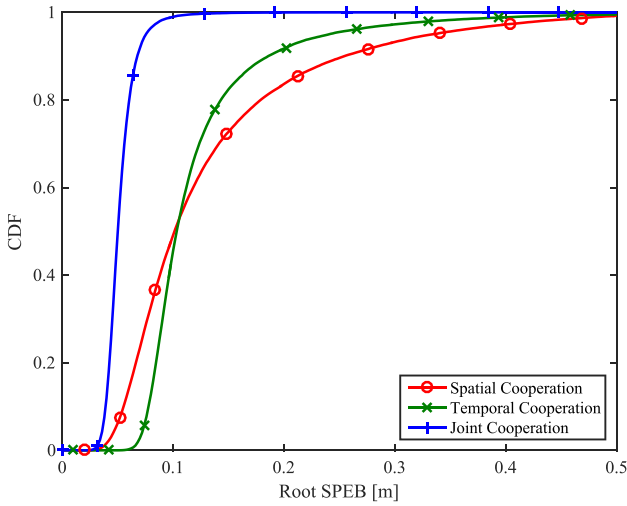


Fig. 11. CDF of the root SPEB in a cooperative network with four agents at the third instant.

set of 36 anchors and several agents. The group of agents move together along a circular trajectory centered at [250 m, 250 m] with radius 150 m, and at each instant the group of agents are placed randomly in a 50-m by 50-m area, whose center is on the circular trajectory. Moreover, the standard deviation of the intra-node measurement error of each agent is set to 0.05 m, and consider that the noises at different time slots are independent for simplicity. Each anchor-agent measurement is made using the OFDM signals with 1-mW power, 10-MHz bandwidth, and 2-GHz carrier frequency, whereas each agent-agent measurement is with 0.1-mW power.

Fig. 10(a) depicts the average root SPEB as a function of the instant under different modes of cooperation for a fouragent network. As a baseline with only measurements from anchors, the average root SPEB is equal to 0.31 m. First, with only spatial cooperation, the average root SPEB decreases to 0.093 m, i.e., a 70% error reduction from the baseline. Note that with only spatial cooperation, the performance does not change over the time. This is because no intra-node measurements are available to carry over the location information in time, and the agents locate themselves independently at different instants using only the inter-node measurements. Second, with only temporal cooperation, the root SPEB decreases significantly with the instants, owing to the contribution from the carry-over information. Since the carry-over information is upper bounded by the information from intra-node measurements, the root SPEB eventually converges to a steady value around 0.042 m, i.e., an approximately 85% error reduction from the baseline. Finally, joint spatial and temporal cooperation further decreases the root SPEB to 0.022 m, i.e., an approximately 90% error reduction from the baseline.

As a counterpart, Fig. 10(b) depicts the average root SPEB as a function of the number of agents under

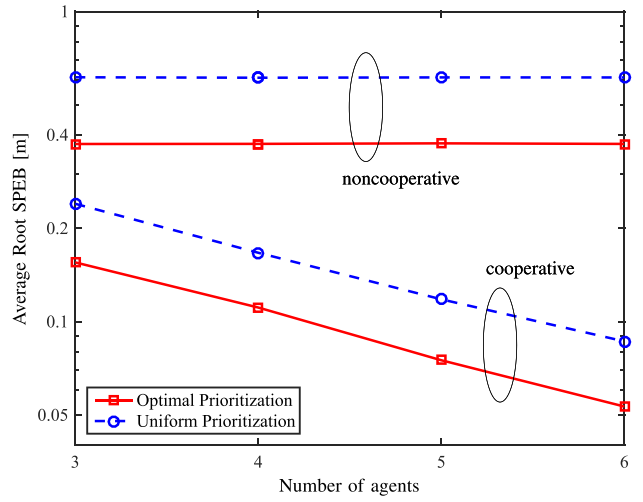


Fig. 12. Average root SPEB as a function of the number of agents through the optimal and uniform node prioritization in a static network.

different modes of cooperation at the third instant. First, with only temporal cooperation, the average root SPEB does not change with the number of agents, as each agent independently localizes itself. Second, with only spatial cooperation, the root SPEB decreases with the number of agents as expected from the theory. For example, the root SPEB is roughly 0.036 m, i.e., an approximately 90% error reduction from the baseline, when there are eight agents in spatial cooperation, and it further decreases to 0.016 m, i.e., an approximately 95% error reduction from the baseline, with spatiotemporal cooperation.

Fig. 11 depicts the cumulative distribution function (CDF) of the root SPEB in a network with four agents at the third instant under different modes of cooperation. The spatiotemporal cooperation scheme outperforms either spatialonly or temporal-only cooperation scheme. As an example, the 95th percentiles of the root SPEB are 0.33, 0.24, and 0.075 m, corresponding to spatial, temporal, and spatiotemporal cooperation, respectively.

In summary, this set of results quantifies the contributions from different modes of cooperation for localization, and shows how the network size in space and the carry-over information in time affect the localization accuracy. These results provide insights into the benefit of spatial and temporal cooperation, which are useful for the design of cooperative systems.

D. Insights into Network Operation

Finally, we will show how the theoretical foundation of NLN guides the design of network operation strategies through two representative cases: node prioritization [173]–[175] and node activation [176]–[178] in the network for localization.

The goal of node prioritization is to achieve the best localization accuracy for a given total transmission power or bandwidth. In particular, for the static scenario, the problem translates to allocating the total transmission power to anchors so that the average SPEB of the agents is minimized. The optimal solution for the node prioritization can be achieved by convex optimization programs thanks to the amenable properties of the SPEB [173]. As a baseline for comparison, we also adopt the uniform power allocation. The signal bandwidth is 10 MHz, and the total power to be allocated among anchors is N_a mW, and in the cooperative case each agent-agent ranging measurement consumes additional 0.1 mW. Fig. 12 depicts the average root SPEB of the agents as a function of the number of agents. First, in the cooperative case, the average root SPEB decreases with the number of agents since more degrees of freedom are available for node prioritization and additional agent-agent measurements are available. Second, the optimal prioritization yields a much better localization performance than the uniform prioritization. For example, in the noncooperative case, the former is 0.37 m while the latter is 0.61 m, which constitutes an approximately 40% error reduction. Third, the spatial cooperation among the agents further improves the localization performance with the same amount of total power from the anchors. For the case of four agents in cooperation, the root SPEB reduces to 0.11 and 0.17 m with the optimal and uniform prioritization, both yielding an approximately 70% error reduction from their noncooperative counterparts. We also present the node activation as an example for the dynamic scenarios. The goal of node activation is to select the best pairs of nodes for inter-node measurements at each instant so that the localization error of the entire network is minimized. The solution for node activation can be obtained either by opportunistic activation or by simply random activation with different tradeoffs between the performance and communication overheads [176].²³ Fig. 13 depicts the average root SPEB of the agents as a function of the number of measurement pairs at each instant, where the network has two or six agents and the standard deviation of the intra-node measurement error of each agent is set to 0.05 m. Moreover, for a fair comparison, the total transmission power of the network is fixed to be N_a mW, and thus more measurement pairs result in less signal power for each measurement pair. First, the average root SPEB decreases with the number of measurement pairs for both opportunistic and random activation as expected, since more degrees of freedom are available for node activation although the total transmission power is fixed. However, the additional gain diminishes as the number of measurement pairs grows, since the degree of freedom is fully exploited. Second, the opportunistic activation can achieve

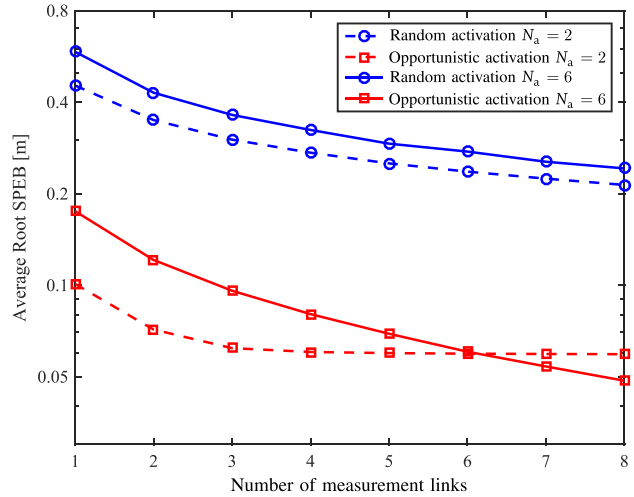


Fig. 13. Average root SPEB through the opportunistic and random activation in a dynamic network. The network consists of two or six agents that are randomly placed in the area.

a much better performance than its random counterparts. For instance, for the case of six agents in the network employing five measurement pairs at each instant, the root SPEB is 0.069 and 0.293 m for opportunistic and random activation, respectively. That is, a 75% reduction in the root SPEB can be achieved by the former method. Third, the opportunistic activation can yield better localization performance when there are more agents in the network with sufficient measurement links. In this case, mobile agents will not only have more opportunities to access anchors, but also increase the diversity for selecting nodes, both of which can potentially provide more information for localization.

In summary, these results demonstrate that the optimized node prioritization and node activation can significantly improve the localization performance under resource constraints. Meanwhile, with the aid of the theoretical results, we can optimize the performance of the location-aware networks in an efficient way.

VIII. CONCLUSION

Location awareness is a key enabler for mobile network applications, spanning from location-based services to autonomous vehicles, which require different levels of localization accuracy and reliability. Network localization and navigation (NLN) enabled by spatiotemporal cooperation is a promising paradigm that can dramatically improve the localization performance. This paper presented a comprehensive exploration of theoretical foundation, where the methodology of equivalent Fisher information analysis was applied to determine the fundamental limits of localization accuracy attainable by spatiotemporal cooperation. The effects of spatiotemporal cooperation, the antenna arrays, and map exploitation were characterized on the localization performance, and a geometric interpretation

²³The opportunistic activation selects the best set of links for reducing the SPEB at each instant, while the random activation selects a number of links from available measurement pairs uniformly.

was developed to visualize the information dynamics in NLN. These results and the insights can be used to guide the algorithm and network design for NLN.

Despite the recent advances in the field, there are still several open challenges to be addressed for NLN. In particular, low-cost solutions for information fusion need to be developed for high-accuracy localization in harsh environments. Also needed is the design of efficient communication protocols that can guarantee the efficiency and

reliability of NLN. In addition, security and privacy are critical issues especially for homeland security and military applications, which needs further study. □

IX. ACKNOWLEDGMENT

The authors would like to thank A. Conti, G. C. Ferrante, A. Giorgetti, Z. Liu, and S. Mazuelas for their helpful suggestions and careful reading of the manuscript.

REFERENCES

- [1] M. Z. Win et al., "Network localization and navigation via cooperation," *IEEE Commun. Mag.*, vol. 49, no. 5, pp. 56–62, May 2011.
- [2] N. Bulusu, J. Heidemann, and D. Estrin, "GPS-less low-cost outdoor localization for very small devices," *IEEE Pers. Commun.*, vol. 7, no. 5, pp. 28–34, Oct. 2000.
- [3] D. Schneider, "New indoor navigation technologies work where GPS can't," *IEEE Spectrum*, Nov. 2013.
- [4] S. Gezici et al., "Localization via ultra-wideband radios: A look at positioning aspects for future sensor networks," *IEEE Signal Process. Mag.*, vol. 22, no. 4, pp. 70–84, Jul. 2005.
- [5] Y. Shen and M. Z. Win, "Fundamental limits of wideband localization—Part I: A general framework," *IEEE Trans. Inf. Theory*, vol. 56, no. 10, pp. 4956–4980, Oct. 2010.
- [6] H. Godrich, A. M. Haimovich, and R. S. Blum, "Target localization accuracy gain in MIMO radar-based systems," *IEEE Trans. Inf. Theory*, vol. 56, no. 6, pp. 2783–2803, Jun. 2010.
- [7] B. T. Robinson, "Who goes there?" *IEEE Spectrum*, vol. 40, no. 10, pp. 42–47, Oct. 2003.
- [8] F. Gustafsson and F. Gunnarsson, "Mobile positioning using wireless networks: Possibilities and fundamental limitations based on available wireless network measurements," *IEEE Signal Process. Mag.*, vol. 22, no. 4, pp. 41–53, Jul. 2005.
- [9] E. Paolini, A. Giorgetti, M. Chiani, R. Minutolo, and M. Montanari, "Localization capability of cooperative anti-intruder radar systems," *EURASIP J. Adv. Signal Process.*, vol. 2008, p. 726854, Dec. 2008.
- [10] J. J. Caffery and G. L. Stuber, "Overview of radiolocation in CDMA cellular systems," *IEEE Commun. Mag.*, vol. 36, no. 4, pp. 38–45, Apr. 1998.
- [11] K. Pahlavan, X. Li, and J.-P. Mäkelä, "Indoor geolocation science and technology," *IEEE Commun. Mag.*, vol. 40, no. 2, pp. 112–118, Feb. 2002.
- [12] K. Yu, J.-P. Montillet, A. Rabbachin, P. Cheong, and I. Oppermann, "UWB location and tracking for wireless embedded networks," *Signal Process.*, vol. 86, no. 9, pp. 2153–2171, 2006.
- [13] J. Warrior, E. McHenry, and K. McGee, "They know where you are—Location detection," *IEEE Spectrum*, vol. 40, no. 7, pp. 20–25, 2003.
- [14] L.-J. Kau and C.-S. Chen, "A smart phone-based pocket fall accident detection, positioning, and rescue system," *IEEE J. Biomed. Health Inf.*, vol. 19, no. 1, pp. 44–56, Jan. 2015.
- [15] T. Latif, E. Whitmire, T. Novak, and A. Borkurt, "Sound localization sensors for search and rescue robots," *IEEE Sensors J.*, vol. 16, no. 10, pp. 3444–3453, May 2016.
- [16] J. Guivant, E. Nebot, and S. Baiker, "Autonomous navigation and map building using laser range sensors in outdoor applications," *J. Robot. Syst.*, vol. 17, no. 10, pp. 565–583, 2000.
- [17] S.-H. Lee and C. C. Chung, "Robust multirate on-road vehicle localization for autonomous highway driving vehicles," *IEEE Trans. Control Syst. Technol.*, vol. 25, no. 2, pp. 577–589, Mar. 2017.
- [18] G. Bresson, Z. Alsayed, L. Yu, and S. Glaser, "Simultaneous localization and mapping: A survey of current trends in autonomous driving," *IEEE Trans. Intell. Vehicles*, vol. 2, no. 3, pp. 194–220, Sep. 2017.
- [19] D. Miorandi, S. Sicari, F. D. Pellegrini, and I. Chlamtac, "Internet of Things: Vision, applications and research challenges," *Ad Hoc Netw.*, vol. 10, no. 7, pp. 1497–1516, Sep. 2012.
- [20] L. Geng, M. F. Bugallo, A. Athalye, and P. M. Djurić, "Indoor tracking with RFID systems," *IEEE J. Sel. Topics Signal Process.*, vol. 8, no. 1, pp. 96–105, Feb. 2014.
- [21] F. Meyer, B. Ertzlinger, Z. Liu, F. Hlawatsch, and M. Z. Win, "A scalable algorithm for network localization and synchronization," *IEEE Internet Things J.*, vol. 5, 2018, to appear.
- [22] T. Budinger, "Biomonitoring with wireless communications," *Annu. Rev. Biomed. Eng.*, vol. 5, no. 1, pp. 383–412, 2003.
- [23] K. Witrals et al., "High-accuracy localization for assisted living: 5G systems will turn multipath channels from foe to friend," *IEEE Signal Process. Mag.*, vol. 33, no. 2, pp. 59–70, Mar. 2016.
- [24] F. Buccafurri, G. Lax, S. Nicolazzo, and A. Nocera, "Robust multirate on-road vehicle localization for autonomous highway driving vehicles," *IEEE Trans. Serv. Comput.*, to be published.
- [25] F. Zabini and A. Conti, "Inhomogeneous Poisson sampling of finite-energy signals with uncertainties in \mathbb{R}^d ," *IEEE Trans. Signal Process.*, vol. 64, no. 18, pp. 4679–4694, Sep. 2016.
- [26] G. Cardone et al., "Fostering participation in smart cities: A geo-social crowdsensing platform," *IEEE Commun. Mag.*, vol. 51, no. 6, pp. 112–119, Jun. 2013.
- [27] S. Bartoletti, A. Conti, and M. Z. Win, "Device-free counting via wideband signals," *IEEE J. Sel. Areas Commun.*, vol. 35, no. 5, pp. 1163–1174, May. 2017.
- [28] B. W. Parkinson and J. J. Spilker, Eds., *Global Positioning System: Theory & Applications* (Progress in Astronautics & Aeronautics), vol. 1. Washington, DC, USA: AIAA, 1996.
- [29] B. W. Parkinson and J. J. Spilker, Eds., *Global Positioning System: Theory and Applications* (Progress in Astronautics and Aeronautics), vol. 2. Washington, DC, USA: AIAA, 1996.
- [30] J. J. Spilker, Jr., "GPS signal structure and performance characteristics," *Navigation*, vol. 25, no. 2, pp. 121–146, Aug. 1978.
- [31] B. W. Parkinson and S. W. Gilbert, "NAVSTAR: Global positioning system—Ten years later," *Proc. IEEE*, vol. 71, no. 10, pp. 1177–1186, Oct. 1983.
- [32] E. Kaplan, Ed., *Understanding GPS: Principles and Applications*. Norwood, MA, USA: Artech House, 1996.
- [33] B. S. Pervan, D. G. Lawrence, and B. W. Parkinson, "Autonomous fault detection and removal using GPS carrier phase," *IEEE Trans. Aerosp. Electron. Syst.*, vol. 34, no. 3, pp. 897–906, Jul. 1998.
- [34] C. J. Hegarty and E. Chatre, "Evolution of the global navigation satellite system (GNSS)," *Proc. IEEE*, vol. 96, no. 12, pp. 1902–1917, Dec. 2008.
- [35] R. W. Klukas, G. Lachapelle, C. Ma, and G.-I. Jee, "GPS signal fading model for urban centres," *IEE Proc. Microw. Antennas Propag.*, vol. 150, no. 4, pp. 245–252, Aug. 2003.
- [36] U. A. Khan, S. Kar, and J. M. F. Moura, "DILAND: An algorithm for distributed sensor localization with noisy distance measurements," *IEEE Trans. Signal Process.*, vol. 58, no. 3, pp. 1940–1947, Mar. 2010.
- [37] A. J. Weiss and A. Amar, "Direct position determination of multiple radio signals," *EURASIP J. Adv. Signal Process.*, vol. 2005, p. 653549, Dec. 2005.
- [38] S. Bartoletti, W. Dai, A. Conti, and M. Z. Win, "A mathematical model for wideband ranging," *IEEE J. Sel. Topics Signal Process.*, vol. 9, no. 2, pp. 216–228, Mar. 2015.
- [39] K. Plarre and P. R. Kumar, "Tracking objects with networked scattered directional sensors," *EURASIP J. Adv. Signal Process.*, vol. 2008, p. 360912, Dec. 2008.
- [40] P. Tichavský, C. H. Muravchik, and A. Nehorai, "Posterior Cramér-Rao bounds for discrete-time nonlinear filtering," *IEEE Trans. Signal Process.*, vol. 46, no. 5, pp. 1386–1396, May 1998.
- [41] S. Safavi, U. Khan, S. Kar, and J. Moura, "Distributed localization: A linear theory," *Proc. IEEE*, vol. 106, no. 7, pp. 1204–1223, Jul. 2018.
- [42] A. M. Haimovich, R. S. Blum, and L. J. Cimini, "MIMO radar with widely separated antennas," *IEEE Signal Process. Mag.*, vol. 25, no. 1, pp. 116–129, Jan. 2008.
- [43] T. V. Nguyen, Y. Jeong, H. Shin, and M. Z. Win, "Machine learning for wideband localization," *IEEE J. Sel. Areas Commun.*, vol. 33, no. 7, pp. 1357–1380, Jul. 2015.
- [44] H. Godrich, A. P. Petropulu, and H. V. Poor, "Power allocation strategies for target localization in distributed multiple-radar architectures," *IEEE Trans. Signal Process.*, vol. 59, no. 7, pp. 3226–3240, Jul. 2011.
- [45] Y. Liu, Y. Shen, D. Guo, and M. Z. Win, "Network localization and synchronization using full-duplex radios," *IEEE Trans. Signal Process.*, vol. 66, no. 3, pp. 714–728, Feb. 2018.
- [46] D. M. Bevy and B. Parkinson, "Cascaded Kalman filters for accurate estimation of multiple biases, dead-reckoning navigation, and full state feedback control of ground vehicles," *IEEE Trans. Control Syst. Technol.*, vol. 15, no. 2, pp. 199–208, Mar. 2007.
- [47] M. Rabinowitz and J. J. Spilker, "A new positioning system using television synchronization signals," *IEEE Trans. Broadcast.*, vol. 51, no. 1, pp. 51–61, Mar. 2005.
- [48] P. Tseng, "Second-order cone programming relaxation of sensor network localization," *SIAM J. Optim.*, vol. 18, no. 1, pp. 156–185, Feb. 2007.
- [49] S. Bartoletti, A. Giorgetti, M. Z. Win, and A. Conti, "Blind selection of representative observations for sensor radar networks," *IEEE Trans. Veh. Technol.*, vol. 64, no. 4, pp. 1388–1400, Apr. 2015.
- [50] O. Bialer, D. Raphaeli, and A. J. Weiss, "Two-way location estimation with synchronized base stations," *IEEE Trans. Signal Process.*, vol. 64, no. 10, pp. 2513–2527, May 2016.
- [51] H. Chen, G. Wang, Z. Wang, H. C. So, and H. V. Poor, "Non-line-of-sight node localization based on semi-definite programming in wireless sensor networks," *IEEE Trans. Wireless Commun.*, vol. 11, no. 1, pp. 108–116, Jan. 2018.
- [52] T. Tirer and A. J. Weiss, "Performance analysis of a high-resolution direct position determination method," *IEEE Trans. Signal Process.*, vol. 65,

- no. 3, pp. 544–554, Feb. 2017.
- [53] F. Meyer et al., “Message passing algorithms for scalable multitarget tracking,” *Proc. IEEE*, vol. 106, no. 2, pp. 221–259, Feb. 2018.
- [54] Y. Shen, H. Wymeersch, and M. Z. Win, “Fundamental limits of wideband localization—Part II: Cooperative networks,” *IEEE Trans. Inf. Theory*, vol. 56, no. 10, pp. 4981–5000, Oct. 2010.
- [55] Y. Shen, S. Mazuelas, and M. Z. Win, “Network navigation: Theory and interpretation,” *IEEE J. Sel. Areas Commun.*, vol. 30, no. 9, pp. 1823–1834, Oct. 2012.
- [56] H. Wymeersch, J. Lien, and M. Z. Win, “Cooperative localization in wireless networks,” *Proc. IEEE*, vol. 97, no. 2, pp. 427–450, Feb. 2009.
- [57] N. Patwari, J. N. Ash, S. Kyperountas, A. O. Hero, R. L. Moses, and N. S. Correal, “Locating the nodes: Cooperative localization in wireless sensor networks,” *IEEE Signal Process. Mag.*, vol. 22, no. 4, pp. 54–69, Jul. 2005.
- [58] A. Conti, D. Dardari, M. Guerra, L. Mucchi, and M. Z. Win, “Experimental characterization of diversity navigation,” *IEEE Syst. J.*, vol. 8, no. 1, pp. 115–124, Mar. 2014.
- [59] H. Wymeersch, S. Marano, W. M. Gifford, and M. Z. Win, “A machine learning approach to ranging error mitigation for UWB localization,” *IEEE Trans. Commun.*, vol. 60, no. 6, pp. 1719–1728, Jun. 2012.
- [60] J. Xu, X. Shen, J. W. Mark, and J. Cai, “Mobile location estimation in CDMA cellular networks by using fuzzy logic,” *Wireless Commun. Mobile Comput.*, vol. 7, no. 3, pp. 285–298, Mar. 2007.
- [61] D. Dardari, A. Conti, U. Ferner, A. Giorgetti, and M. Z. Win, “Ranging with ultrawide bandwidth signals in multipath environments,” *Proc. IEEE*, vol. 97, no. 2, pp. 404–426, Feb. 2009.
- [62] B. Denis, J.-B. Pierrot, and C. Abou-Rjeily, “Joint distributed synchronization and positioning in UWB ad hoc networks using TOA,” *IEEE Trans. Microw. Theory Techn.*, vol. 54, no. 4, pp. 1896–1911, Jun. 2006.
- [63] S. Mazuelas, A. Conti, J. C. Allen, and M. Z. Win, “Soft range information for network localization,” *IEEE Trans. Signal Process.*, vol. 66, no. 12, pp. 3155–3168, Jun. 2018.
- [64] A. Ohya, A. Kosaka, and A. Kak, “Vision-based navigation by a mobile robot with obstacle avoidance using single-camera vision and ultrasonic sensing,” *IEEE Trans. Robot. Autom.*, vol. 14, no. 6, pp. 969–978, Dec. 1998.
- [65] J. A. Castellanos, J. Neira, and J. D. Tardos, “Multisensor fusion for simultaneous localization and map building,” *IEEE Trans. Robot. Autom.*, vol. 17, no. 6, pp. 908–914, Dec. 2001.
- [66] A. I. Mourikis, N. Trawny, S. I. Roumeliotis, A. E. Johnson, A. Ansar, and L. Matthies, “Vision-Aided Inertial Navigation for Spacecraft Entry, Descent, and Landing,” *IEEE Trans. Robot.*, vol. 25, no. 2, pp. 264–280, Apr. 2009.
- [67] W. Burgard, O. Brock, and C. Stachniss, “Map-based precision vehicle localization in urban environments,” in *Proc. Robot. Sci. Syst. Conf.*, Baden-Baden, Germany, Jun. 2007, pp. 121–128.
- [68] J. Levinson et al., “Towards fully autonomous driving: Systems and algorithms,” in *Proc. IEEE Intell. Vehicles Symp. (IV)*, Baden-Baden, Germany, Jun. 2011, pp. 163–168.
- [69] R. W. Wolcott and R. M. Eustice, “Visual localization within LIDAR maps for automated urban driving,” in *Proc. IEEE/RSJ Int. Conf. Intell. Robots Syst.*, Chicago, IL, USA, Sep. 2014, pp. 176–183.
- [70] P. Lazik, N. Rajagopal, O. Shih, B. Sinopoli, and A. Rowe, “ALPS: A Bluetooth and ultrasound platform for mapping and localization,” in *Proc. Conf. Embedded Networked Sensor Syst.*, Seoul, South Korea, 2015, pp. 73–84.
- [71] N. B. Priyantha, A. Chakraborty, and H. Balakrishnan, “The cricket location-support system,” in *Proc. 6th Annu. Int. Conf. Mobile Comput. Netw.* New York, NY, USA: 2000, pp. 32–43.
- [72] Z. Liu, W. Dai, and M. Z. Win, “Mercury: An infrastructure-free system for network localization and navigation,” *IEEE Trans. Mobile Comput.*, vol. 17, no. 5, pp. 1119–1133, May 2018.
- [73] U. A. Khan, S. Kar, and J. M. F. Moura, “Distributed sensor localization in random environments using minimal number of anchor nodes,” *IEEE Trans. Signal Process.*, vol. 57, no. 5, pp. 2000–2016, May 2009.
- [74] M. Z. Win and Y. Shen, “On the accuracy of localization systems using wideband antenna arrays,” *IEEE Trans. Commun.*, vol. 58, no. 1, pp. 270–280, Jan. 2010.
- [75] A. H. Sayed, A. Tarighat, and N. Khajepourni, “Network-based wireless location: Challenges faced in developing techniques for accurate wireless location information,” *IEEE Signal Process. Mag.*, vol. 22, no. 4, pp. 24–40, Jul. 2005.
- [76] J. Prieto, S. Mazuelas, and M. Z. Win, “Context-aided inertial navigation via belief condensation,” *IEEE Trans. Signal Process.*, vol. 64, no. 12, pp. 3250–3261, Jun. 2016.
- [77] P. D. Groves, *Principles of GNSS, Inertial, and Multisensor Integrated Navigation Systems*. Norwood, MA, USA: Artech House, 2008.
- [78] A. R. J. Ruiz, F. S. Granja, J. C. P. Honorato, and J. I. G. Rosas, “Accurate pedestrian indoor navigation by tightly coupling foot-mounted IMU and RFID measurements,” *IEEE Trans. Instrum. Meas.*, vol. 61, no. 1, pp. 178–189, Jan. 2012.
- [79] S. Beauregard, “A helmet-mounted pedestrian dead reckoning system,” in *Proc. 3rd Int. Forum Appl. Wearable Comput.*, Mar. 2006, pp. 1–11.
- [80] S. Mazuelas, Y. Shen, and M. Z. Win, “Belief condensation filtering,” *IEEE Trans. Signal Process.*, vol. 61, no. 18, pp. 4403–4415, Sep. 2013.
- [81] E. Foxlin, “Pedestrian tracking with shoe-mounted inertial sensors,” *IEEE Comput. Graph. Appl.*, vol. 25, no. 6, pp. 38–46, Nov./Dec. 2005.
- [82] J. Wolf, W. Burgard, and H. Burkhardt, “Robust vision-based localization by combining an image-retrieval system with Monte Carlo localization,” *IEEE Trans. Robot.*, vol. 21, no. 2, pp. 208–216, Apr. 2005.
- [83] S. Se, D. G. Lowe, and J. J. Little, “Vision-based global localization and mapping for mobile robots,” *IEEE Trans. Robot.*, vol. 21, no. 3, pp. 364–375, Jun. 2005.
- [84] A. J. Davison and D. W. Murray, “Simultaneous localization and map-building using active vision,” *IEEE Trans. Pattern Anal. Mach. Intell.*, vol. 24, no. 7, pp. 865–880, Jul. 2002.
- [85] A. Georgiev and P. K. Allen, “Localization methods for a mobile robot in urban environments,” *IEEE Trans. Robot.*, vol. 20, no. 5, pp. 851–864, Oct. 2004.
- [86] A. Conti, M. Guerra, D. Dardari, N. Decarli, and M. Z. Win, “Network experimentation for cooperative localization,” *IEEE J. Sel. Areas Commun.*, vol. 30, no. 2, pp. 467–475, Feb. 2012.
- [87] M. Anisetti, C. A. Ardagna, V. Bellandi, E. Damiani, and S. Reale, “Map-based location and tracking in multipath outdoor mobile networks,” *IEEE Trans. Wireless Commun.*, vol. 10, no. 3, pp. 814–824, Mar. 2011.
- [88] Y. Cheng and T. Singh, “Efficient particle filtering for road-constrained target tracking,” *IEEE Trans. Aerosp. Electron. Syst.*, vol. 43, no. 4, pp. 1454–1469, Oct. 2007.
- [89] F. Montorsi, S. Mazuelas, G. M. Vitetta, and M. Z. Win, “On the performance limits of map-aware localization,” *IEEE Trans. Inf. Theory*, vol. 59, no. 8, pp. 5023–5038, Aug. 2013.
- [90] K. Zhang, Y. Shen, and M. Z. Win, “On the performance of map-aware cooperative localization,” in *Proc. IEEE Int. Conf. Commun.*, Kuala Lumpur, Malaysia, May 2016, pp. 1–6.
- [91] C. Falsi, D. Dardari, L. Mucchi, and M. Z. Win, “Time of arrival estimation for UWB localizers in realistic environments,” *EURASIP J. Appl. Signal Process.*, vol. 2006, Article ID 32 082, 2006.
- [92] A. Rabbachin, I. Oppermann, and B. Denis, “GML ToA estimation based on low complexity UWB energy detection,” in *Proc. PIMRC, Helsinki*, Finland, Sep. 2006, pp. 1–5.
- [93] D. Dardari, C.-C. Chong, and M. Z. Win, “Threshold-based time-of-arrival estimators in UWB dense multipath channels,” *IEEE Trans. Commun.*, vol. 56, no. 8, pp. 1366–1378, Aug. 2008.
- [94] Z. N. Low, J. H. Cheong, C. L. Law, W. T. Ng, and Y. J. Lee, “Pulse detection algorithm for line-of-sight (LOS) UWB ranging applications,” *IEEE Antennas Wireless Propag. Lett.*, vol. 4, pp. 63–67, 2005.
- [95] Z. Zhang, C. L. Law, and Y. L. Guan, “BA-POC-based ranging method with multipath mitigation,” *IEEE Antennas Wireless Propag. Lett.*, vol. 4, no. 1, pp. 492–495, 2005.
- [96] M. Leng, W. P. Tay, C. M. S. See, S. G. Razul, and M. Z. Win, “Modified CRLB for cooperative geolocation of two devices using signals of opportunity,” *IEEE Trans. Wireless Commun.*, vol. 13, no. 7, pp. 3636–3649, Jul. 2014.
- [97] T. Wang, Y. Shen, S. Mazuelas, H. Shin, and M. Z. Win, “On OFDM ranging accuracy in multipath channels,” *IEEE Syst. J.*, vol. 8, no. 1, pp. 104–114, Mar. 2014.
- [98] J. Caffery, *Wireless Location in CDMA Cellular Radio Systems*. Boston, MA, USA: Kluwer, 2000.
- [99] T. S. Rappaport, J. Reed, and B. D. Woerner, “Position location using wireless communications on highways of the future,” *IEEE Commun. Mag.*, vol. 34, no. 10, pp. 33–41, Oct. 1996.
- [100] W. W.-L. Li, Y. Shen, Y. J. Zhang, and M. Z. Win, “Robust power allocation for energy-efficient location-aware networks,” *IEEE/ACM Trans. Netw.*, vol. 21, no. 6, pp. 1918–1930, Dec. 2013.
- [101] H.-S. Ahn and W. Yu, “Environmental-adaptive RSSI-based indoor localization,” *IEEE Trans. Autom. Sci. Eng.*, vol. 6, no. 4, pp. 626–633, Oct. 2009.
- [102] N. Patwari and A. O. Hero, III, “Using proximity and quantized RSS for sensor localization in wireless networks,” *Proc. IEEE/ACM 2nd Workshop Wireless Sensor Nets. Appl.*, 2003, pp. 20–29.
- [103] T. Pavan, G. Costa, M. Mazzotti, A. Conti, and D. Dardari, “Experimental results on indoor localization techniques through wireless sensors network,” in *Proc. IEEE Semiannu. Veh. Technol. Conf.*, vol. 2, Melbourne, Australia, May 2006, pp. 663–667.
- [104] J. P. Beaudeau, M. F. Bugallo, and P. M. Djurić, “RSSI-based multi-target tracking by cooperative agents using fusion of cross-target information,” *IEEE Trans. Signal Process.*, vol. 63, no. 19, pp. 5033–5044, Oct. 2015.
- [105] P. Bahl and V. N. Padmanabhan, “RADAR: An in-building RF-based user location and tracking system,” in *Proc. INFOCOM*, vol. 2, Tel Aviv, Israel, Mar. 2000, pp. 775–784.
- [106] Y. Shang, W. Rumi, Y. Zhang, and M. Fromherz, “Localization from connectivity in sensor networks,” *IEEE Trans. Parallel Distrib. Syst.*, vol. 15, no. 11, pp. 961–974, Nov. 2004.
- [107] T. He, C. Huang, B. M. Blum, J. A. Stankovic, and T. Abdelzaher, “Range-free localization schemes for large scale sensor networks,” in *Proc. 9th Annu. Int. Conf. Mobile Comput. Netw.*, New York, NY, USA, 2003, pp. 81–95.
- [108] M. Li and Y. Liu, “Rendered path: Range-free localization in anisotropic sensor networks with holes,” *IEEE/ACM Trans. Netw.*, vol. 18, no. 1, pp. 320–332, Feb. 2010.
- [109] T.-J. Shan, M. Wax, and T. Kailath, “On spatial smoothing for direction-of-arrival estimation of coherent signals,” *IEEE Trans. Acoust. Speech Signal Process.*, vol. 33, no. 4, pp. 806–811, Apr. 1985.
- [110] B. D. V. Veen and K. M. Buckley, “Beamforming: A versatile approach to spatial filtering,” *IEEE ASSP Mag.*, vol. 5, no. 2, pp. 4–24, Apr. 1988.
- [111] H. Krim and M. Viberg, “Two decades of array signal processing research: The parametric approach,” *IEEE Signal Process. Mag.*, vol. 13, no. 4, pp. 67–94, Jul. 1996.
- [112] R. Engelbrecht, “Passive source localization from spatially correlated angle-of-arrival data,” *IEEE Trans. Acoust. Speech Signal Process.*, vol. 31, no. 4, pp. 842–846, Aug. 1983.
- [113] M. Wax and T. Kailath, “Optimum localization of

- multiple sources by passive arrays," *IEEE/ACM Trans. Audio Speech Language Process.*, vol. 31, no. 5, pp. 1210–1217, Oct. 1983.
- [114] R. Roy and T. Kailath, "ESPRIT-estimation of signal parameters via rotational invariance techniques," *IEEE/ACM Trans. Audio Speech Language Process.*, vol. 37, no. 7, pp. 984–995, Jul. 1989.
- [115] C.-C. Chong, C.-M. Tan, D. I. Laurenson, S. McLaughlin, M. A. Beach, and A. R. Nix, "A new statistical wideband spatio-temporal channel model for 5-GHz band WLAN systems," *IEEE J. Sel. Areas Commun.*, vol. 21, no. 2, pp. 139–150, Feb. 2003.
- [116] D. Niculescu and B. Nath, "Ad hoc positioning system (APS) using AOA," in *Proc. 22nd Annu. Joint Conf. IEEE Comput. Commun.*, vol. 3. San Francisco, CA, USA, Mar./Apr. 2003, pp. 1734–1743.
- [117] L. Xiong, "A selective model to suppress NLOS signals in angle-of-arrival (AOA) location estimation," in *Proc. 9th IEEE Int. Symp. Pers. Indoor Mobile Radio Commun.*, vol. Sep. 1, 1998, pp. 461–465.
- [118] H.-J. Shao, X.-P. Zhang, and Z. Wang, "Efficient closed-form algorithms for AOA based self-localization of sensor nodes using auxiliary variables," *IEEE Trans. Signal Process.*, vol. 62, no. 10, pp. 2580–2594, May 2014.
- [119] A. F. Molisch, *Wireless Communications*, 1st ed. Piscataway, NJ, USA: Wiley, 2005.
- [120] C.-Y. Lee, "Finding the approximate angular probability density function of wave arrival by using a directional antenna," *IEEE Trans. Antennas Propag.*, vol. 21, no. 3, pp. 328–334, May 1973.
- [121] B. Zhang and F. Yu, "LSWD: Localization scheme for wireless sensor networks using directional antenna," *IEEE Trans. Consum. Electron.*, vol. 56, no. 4, pp. 2208–2216, Nov. 2010.
- [122] T. V. Nguyen, Y. Jeong, H. Shin, and M. Z. Win, "Least square cooperative localization," *IEEE Trans. Veh. Technol.*, vol. 64, no. 4, pp. 1318–1330, Apr. 2015.
- [123] J. Luo and Q. Zhang, "Relative distance based localization for mobile sensor networks," in *Proc. IEEE Global Telecomm. Conf.*, DC, USA, Nov. 2007, pp. 1076–1080.
- [124] J. Chen, W. Dai, Y. Shen, V. K. N. Lau, and M. Z. Win, "Resource management games for distributed network localization," *IEEE J. Sel. Areas Commun.*, vol. 35, no. 2, pp. 317–329, Feb. 2017.
- [125] S. Safavi and U. A. Khan, "An opportunistic linear-convex algorithm for localization in mobile robot networks," *IEEE Trans. Robot.*, vol. 33, no. 4, pp. 875–888, Aug. 2017.
- [126] S. Safavi and U. A. Khan, "Localization in mobile networks via virtual convex hulls," *IEEE Trans. Signal Inf. Process. Netw.*, vol. 4, no. 1, pp. 188–201, Mar. 2018.
- [127] W. Chen and X. Meng, "A cooperative localization scheme for zigbee-based wireless sensor networks," in *Proc. 14th IEEE Int. Conf. Netw.*, Singapore, Sep. 2006, pp. 1–5.
- [128] N. Alsindi and K. Pahlavan, "Cooperative localization bounds for indoor ultra-wideband wireless sensor networks," *EURASIP J. Adv. Signal Process.*, vol. Jan. 2008, 2008, no. 125.
- [129] C. Savarese, J. M. Rabaey, and J. Beutel, "Locationing in distributed ad-hoc wireless sensor networks," in *Proc. IEEE Int. Conf. Acoust. Speech Signal Process.*, vol. May 4, 2001, pp. 2037–2040.
- [130] W. Dai, Y. Shen, and M. Z. Win, "Distributed power allocation for cooperative wireless network localization," *IEEE J. Sel. Areas Commun.*, vol. 33, no. 1, pp. 28–40, Jan. 2015.
- [131] X. Tan and J. Li, "Cooperative positioning in underwater sensor networks," *IEEE Trans. Signal Process.*, vol. 58, no. 11, pp. 5860–5871, Nov. 2010.
- [132] R. M. Vaghefi, M. R. Gholami, R. M. Buehrer, and E. G. Ström, "Cooperative received signal strength-based sensor localization with unknown transmit powers," *IEEE Trans. Signal Process.*, vol. 61, no. 6, pp. 1389–1403, Mar. 2013.
- [133] J. Chen, W. Dai, Y. Shen, V. K. N. Lau, and M. Z. Win, "Power management for cooperative localization: A game theoretical approach," *IEEE Trans. Signal Process.*, vol. 64, no. 24, pp. 6517–6532, Dec. 2016.
- [134] C. Chang and A. Sahai, "Cramér-Rao-type bounds for localization," *EURASIP J. Appl. Signal Process.*, vol. Dec. 2006, 2006, no. 094287.
- [135] S. B. Cruz, T. E. Abrudan, Z. Xiao, N. Trigoni, and J. Barros, "Neighbor-aided localization in vehicular networks," *IEEE Trans. Intell. Transp. Syst.*, vol. 18, no. 10, pp. 2693–2702, Oct. 2017.
- [136] J. Yao, A. T. Balaei, M. Hassan, N. Alam, and A. G. Dempster, "Improving cooperative positioning for vehicular networks," *IEEE Trans. Veh. Technol.*, vol. 60, no. 6, pp. 2810–2823, Jul. 2011.
- [137] U. A. Khan and J. M. F. Moura, "Distributing the Kalman filter for large-scale systems," *IEEE Trans. Signal Process.*, vol. 56, no. 10, pp. 4919–4935, Oct. 2008.
- [138] S. Mazuelas, Y. Shen, and M. Z. Win, "Information coupling in cooperative localization," *IEEE Commun. Lett.*, vol. 15, no. 7, pp. 737–739, Jul. 2011.
- [139] S. Mazuelas, Y. Shen, and M. Z. Win, "Spatio-temporal information coupling in network navigation," *IEEE Trans. Inf. Theory*, vol. 64, 2018, to appear.
- [140] H. L. Van Trees and K. L. Bell, *Detection Estimation and Modulation Theory, Part 1*. New York, NY: Wiley, 1968.
- [141] H. V. Poor, *An Introduction to Signal Detection and Estimation*, 2nd ed. New York, NY, USA: Springer-Verlag, 1994.
- [142] T. M. Cover and J. A. Thomas, *Elements of Information Theory*, 2nd ed. Hoboken, NJ, USA: Wiley, 2006.
- [143] F. Gini, R. Reggiannini, and U. Mengali, "The modified Cramér–Rao bound in vector parameter estimation," *IEEE Trans. Commun.*, vol. 46, no. 1, pp. 52–60, Jan. 1998.
- [144] I. Reuven and H. Messer, "A Barankin-type lower bound on the estimation error of a hybrid parameter vector," *IEEE Trans. Inf. Theory*, vol. 43, no. 3, pp. 1084–1093, May 1997.
- [145] J. Ziv and M. Zakai, "Some lower bounds on signal parameter estimation," *IEEE Trans. Inf. Theory*, vol. 15, no. 3, pp. 386–391, May. 1969.
- [146] M. Zakai and J. Ziv, "On the threshold effect in radar range estimation," *IEEE Trans. Inf. Theory*, vol. IT-15, no. 1, pp. 167–170, Jan. 1969.
- [147] D. Chazan, M. Zakai, and J. Ziv, "Improved lower bounds on signal parameter estimation," *IEEE Trans. Inf. Theory*, vol. 21, no. 1, pp. 90–93, Jan. 1975.
- [148] K. L. Bell, Y. Steinberg, Y. Ephraim, and H. L. V. Trees, "Extended Ziv-Zakai lower bound for vector parameter estimation," *IEEE Trans. Inf. Theory*, vol. 43, no. 2, pp. 624–637, Mar. 1997.
- [149] E. Weinstein and A. J. Weiss, "A general class of lower bounds in parameter estimation," *IEEE Trans. Inf. Theory*, vol. 34, no. 2, pp. 338–342, Mar. 1988.
- [150] C. Chang and A. Sahai, "Estimation bounds for localization," in *Proc. IEEE Commun. Soc. Conf. Sensor Ad Hoc Commun. Netw. (SECON)*, Oct. 2004, pp. 415–424.
- [151] L. Maillaender, "On the geolocation bounds for round-trip time-of-arrival and all non-line-of-sight channels," *EURASIP J. Adv. Signal Process.*, vol. Dec. 2008, 2008, no. 584670.
- [152] Y. Qi, H. Kobayashi, and H. Suda, "Analysis of wireless geolocation in a non-line-of-sight environment," *IEEE Trans. Wireless Commun.*, vol. 5, no. 3, pp. 672–681, Mar. 2006.
- [153] D. Jourdan, D. Dardari, and M. Win, "Position error bound for UWB localization in dense cluttered environments," *IEEE Trans. Aerosp. Electron. Syst.*, vol. 44, no. 2, pp. 613–628, Apr. 2008.
- [154] S. Venkatesh and R. M. Buehrer, "Multiple-access insights from bounds on sensor localization," *Pervasive Mobile Comput.*, vol. 4, no. 1, pp. 33–61, 2008.
- [155] S. Mazuelas, R. M. Lorenzo, A. Bahillo, P. Fernandez, J. Prieto, and E. J. Abril, "Topology assessment provided by weighted barycentric parameters in harsh environment wireless location systems," *IEEE Trans. Signal Process.*, vol. 58, no. 7, pp. 3842–3857, Jul. 2010.
- [156] Y. Qi and H. Kobayashi, "Cramér-Rao lower bound for geolocation in non-line-of-sight environment," in *Proc. IEEE Int. Conf. Acoust. Speech Signal Process.*, Orlando, FL, USA, May 2002, pp. III-2473–III-2476.
- [157] Y. Qi, H. Suda, and H. Kobayashi, "On time-of-arrival positioning in a multipath environment," in *Proc. IEEE Semiannu. Veh. Technol. Conf.*, Los Angeles, CA, USA, Sep. 2004, pp. 3540–3544.
- [158] Y. Shen and M. Z. Win, "Fundamental limits of wideband localization accuracy via Fisher information," in *Proc. IEEE Wireless Commun. Netw. Conf.*, Kowloon, China, Mar. 2007, pp. 3046–3051.
- [159] Y. Han et al., "Performance limits and geometric properties of array localization," *IEEE Trans. Inf. Theory*, vol. 62, no. 2, pp. 1054–1075, Feb. 2016.
- [160] O. Cappe, E. Moulines, and T. Ryden, *Inference in Hidden Markov Models*, ser. Statistics. New York, NY, USA: Springer-Verlag, 2007.
- [161] L. R. Rabiner, "A tutorial on hidden Markov models and selected applications in speech recognition," *Proc. IEEE*, vol. 77, no. 2, pp. 257–286, Feb. 1989.
- [162] L. Rabiner and B. Juang, "An introduction to hidden Markov models," *IEEE ASSP Mag.*, vol. 3, no. 1, pp. 4–16, Jan. 1986.
- [163] T. Kailath, A. H. Sayed, and B. Hassibi, *Linear Estimation*, ser. Information and System Sciences. Upper Saddle River, NJ, USA: Prentice-Hall, 2000.
- [164] S. Bay, B. Geller, A. Renaux, J.-P. Barbot, and J.-M. Brossier, "On the hybrid Cramér Rao bound and its application to dynamical phase estimation," *IEEE Wireless Commun. Lett.*, vol. 15, no. 8, pp. 453–456, May 2008.
- [165] A. T. Ihler, J. W. Fisher, R. L. Moses, and A. S. Willsky, "Nonparametric belief propagation for self-localization of sensor networks," *IEEE J. Sel. Areas Commun.*, vol. 23, no. 4, pp. 809–819, Apr. 2005.
- [166] J. Aspnes et al., "A theory of network localization," *IEEE Trans. Mobile Comput.*, vol. 5, no. 12, pp. 1663–1678, Dec. 2006.
- [167] P. Biswas, T.-C. Lian, T.-C. Wang, and Y. Ye, "Semidefinite programming based algorithms for sensor network localization," *ACM Trans. Sensor Netw.*, vol. 2, no. 2, pp. 188–220, 2006.
- [168] S. Mazuelas, Y. Shen, and M. Z. Win, "Spatio-temporal information coupling in cooperative navigation," in *Proc. IEEE Global Telecomm. Conf.*, Anaheim, CA, USA, Dec. 2012, pp. 2403–2407.
- [169] *Technical Specification LTE/Evolved Universal Terrestrial Radio Access (E-UTRA); User Equipment (UE) Radio Transmission and Reception*, document TS 136.101 V11.2.0, 3rd Generation Partnership Project, 3GPP, Nov. 2012.
- [170] *Technical Report LTE; 5G; Study on Channel Model for Frequency Spectrum Above 6 GHz, Release 14*, document ETSI TR 138 900 V14.3.1, 3rd Generation Partnership Project, 3GPP, Aug. 2017.
- [171] F. Ademaj, M. K. Müller, S. Schwarz, and M. Rupp, "Modeling of spatially correlated geometry-based stochastic channel," in *Proc. IEEE Semiannual Veh. Technol. Conf.*, Toronto, ON, Canada, Sep. 2017, pp. 1–6.
- [172] S. Jaeckel, L. Raschkowski, K. Börner, L. Thiele, F. Burkhardt, and E. Eberlein, "Quasi deterministic radio channel generator user manual and documentation," *Fraunhofer Heinrich Hertz Inst.*, Berlin, Germany, Tech. Rep., 2017.
- [173] Y. Shen, W. Dai, and M. Z. Win, "Power optimization for network localization," *IEEE/ACM Trans. Netw.*, vol. 22, no. 4, pp. 1337–1350, Aug. 2014.
- [174] W. Dai, Y. Shen, and M. Z. Win, "Energy-efficient network navigation algorithms," *IEEE J. Sel. Areas Commun.*, vol. 33, no. 7, pp. 1418–1430,

- Jul. 2015.
- [175] W. Dai, Y. Shen, and M. Z. Win, "A computational geometry framework for efficient network localization," *IEEE Trans. Inf. Theory*, vol. 64, no. 2, pp. 1317–1339, Feb. 2018.
- [176] T. Wang, Y. Shen, A. Conti, and M. Z. Win, "Network navigation with scheduling: Error evolution," *IEEE Trans. Inf. Theory*, vol. 63, no. 11, pp. 7509–7534, Nov. 2017.
- [177] T. Wang, Y. Shen, A. Conti, and M. Z. Win, "Analysis of network navigation with scheduling strategies," in *Proc. IEEE Int. Conf. Commun.*, London, U.K., Jun. 2015, pp. 3562–3566.
- [178] M. Z. Win, W. Dai, Y. Shen, G. Christikos, and H. V. Poor, "Network operation strategies for efficient localization and navigation," *Proc. IEEE*, vol. 106, no. 7, pp. 1224–1254, Jul. 2018.

ABOUT THE AUTHORS

Moe Z. Win (Fellow, IEEE) is a Professor at the Massachusetts Institute of Technology (MIT), Cambridge, MA, USA and the founding director of the Wireless Information and Network Sciences Laboratory. Prior to joining MIT, he was with AT&T Research Laboratories and NASA Jet Propulsion Laboratory.

His research encompasses fundamental theories, algorithm design, and network experimentation for a broad range of real-world problems. His current research topics include network localization and navigation, network interference exploitation, and quantum information science. He has served the IEEE Communications Society as an elected Member-at-Large on the Board of Governors, as elected Chair of the Radio Communications Committee, and as an IEEE Distinguished Lecturer. Over the last two decades, he held various editorial positions for IEEE journals and organized numerous international conferences. Currently, he is serving on the SIAM Diversity Advisory Committee.

Dr. Win is an elected Fellow of the American Association for the Advancement of Science (AAAS) and the Institution of Engineering and Technology (IET). He was honored with two IEEE Technical Field Awards: the IEEE Kiyo Tomiyasu Award (2011) and the IEEE Eric E. Sumner Award (2006, jointly with R. A. Scholtz). Together with students and colleagues, his papers have received numerous awards. Other recognitions include the IEEE Communications Society Edwin H. Armstrong Achievement Award (2016), the International Prize for Communications Cristoforo Colombo (2013), the Copernicus Fellowship (2011) and the *Laurea Honoris Causa* (2008) from the Università degli Studi di Ferrara, and the U.S. Presidential Early Career Award for Scientists and Engineers (2004). He is an ISI Highly Cited Researcher.



Yuan Shen (Member, IEEE) received the B.E. degree (with highest honor) in electronic engineering from Tsinghua University, Beijing, China, in 2005 and the S.M. and Ph.D. degrees in electrical engineering and computer science from the Massachusetts Institute of Technology (MIT), Cambridge, MA, USA, in 2008 and 2014, respectively.

He is an Associate Professor at the Department of Electronic Engineering, Tsinghua University. Prior to that, he was a Research Assistant and then Postdoctoral Associate at the Wireless Information and Network Sciences Laboratory, MIT, in 2005–2014. He was with the Hewlett-Packard Labs in winter 2009 and the Corporate R&D at Qualcomm Inc. in summer 2008. His research interests include statistical inference, network science, communication theory, information theory, and optimization. His current research focuses on network localization and navigation, inference techniques, resource allocation, and intrinsic wireless secrecy.



Prof. Shen was a recipient of the Qiu Shi Outstanding Young Scholar Award (2015), the China's Youth 1000-Talent Program (2014), the Marconi Society Paul Baran Young Scholar Award (2010), and the MIT Walter A. Rosenblith Presidential Fellowship (2005). His papers received the IEEE Communications Society Fred W. Ellersick Prize (2012) and three Best Paper Awards from IEEE international conferences. He is an elected Vice Chair (2017–2018) and Secretary (2015–2016) for the IEEE ComSoc Radio Communications Committee. He serves as TPC symposium Co-Chair for IEEE Globecom (2018 and 2016), the European Signal Processing Conference (EUSIPCO 2016), and the IEEE ICC Advanced Network Localization and Navigation (ANLN) Workshop (2016, 2017, and 2018). He also serves as Editor for the IEEE TRANSACTIONS ON WIRELESS COMMUNICATIONS (since 2018), IEEE COMMUNICATIONS LETTERS (since 2015), and IEEE CHINA COMMUNICATIONS (since 2017), and served as Guest Editor for the *International Journal of Distributed Sensor Networks* (in 2015).

Wenhan Dai (Student Member, IEEE) received the B.S. degrees in electronic engineering and in mathematics from Tsinghua University, Beijing, China, in 2011 and the S.M. degree in aeronautics and astronautics from the Massachusetts Institute of Technology (MIT), Cambridge, MA, USA, in 2014, where he is currently working toward the Ph.D. degree at the Wireless Information and Network Sciences Laboratory.

His research interests include communication theory and stochastic optimization with application to wireless communication and network localization. His current research focuses on efficient network localization, cooperative network operation, and ultrawideband communication.

Mr. Dai was honored by the Marconi Society with the Paul Baran Young Scholar Award (2017). He received the Marconi-BISITE Best Paper Award from the IEEE ICUWB (2017), the Chinese Government Award for Outstanding Student Abroad (2016), the first prize of the IEEE Communications Society Student Competition (2016), and the Student Paper Award (first place) from the IEEE CWIT (2015). He was recognized as the exemplary reviewer of IEEE Communications Letters (2014).

